ATTITUDE AND ALTITUDE CONTROL OF A TRIPLE TILT-ROTOR UNMANNED AERIAL VEHICLE

A THESIS SUBMITTED TO

THE GRADUATE SCHOOL OF NATURAL AND APPLIED SCIENCES

OF

ATILIM UNIVERSITY

BY

ALP KAÇAR

IN PARTIAL FULFILLMENT OF THE REQUIREMENTS FOR THE DEGREE OF

MASTER OF SCIENCE

IN

THE DEPARTMENT OF MECHATRONICS ENGINEERING

JULY 2013

Approval of the Graduate School of Natural and Applied Sciences, Atılım University.

_____

Prof. Dr. K. İbrahim AKMAN

Director

I certify that this thesis satisfies all the requirements as a thesis for the degree of Master of Science.

_____

Prof. Dr. Abdülkadir ERDEN

Head of Department

This is to certify that we have read the thesis "Attitude and Altitude Control of a Triple Tilt-Rotor Unmanned Aerial Vehicle" submitted by "Alp KAÇAR" and that in our opinion it is fully adequate, in scope and quality, as a thesis for the degree of Master of Science.

_____	_____
Asst. Prof. Dr. Bülent İRFANOĞLU	Asst. Prof. Dr. Kutluk Bilge ARIKAN
Co-Supervisor	Supervisor

Examining Committee Members

Prof. Dr. Abdülkadir ERDEN	_____
Assoc. Prof. Dr. Sedat NAZLIBİLEK	_____
Asst. Prof. Dr. Ali Emre TURGUT	_____
Asst. Prof. Dr. Bülent İRFANOĞLU	_____
Asst. Prof. Dr. Kutluk Bilge ARIKAN	_____

Date: 19.07.2013

I declare and guarantee that all data, knowledge and information in this document has been obtained, processed and presented in accordance with academic rules and ethical conduct. Based on these rules and conduct, I have fully cited and referenced all material and results that are not original to this work.

Name, Last name: Alp KAÇAR

Signature:

ABSTRACT

ATTITUDE AND ALTITUDE CONTROL OF A TRIPLE TILT-ROTOR UNMANNED AERIAL VEHICLE

Kaçar, Alp

M.S., Mechatronics Engineering Department

Supervisor: Asst. Prof. Dr. Kutluk Bilge Arıkan

Co-Supervisor: Asst. Prof. Dr. Bülent İrfanoğlu

July 2013, - 53 pages

In this thesis, design of triple tilt-rotor unmanned aerial vehicle (UAV) and controller design for attitude and altitude dynamics has been studied. After UAV designed, carbon-fiber bars, plastic parts, tilt mechanisms and landing gears are manufactured. During the manufacturing process; mathematical model is obtained. The model has been linearized to design linear quadratic regulator (LQR) based controllers to stabilize the system and track reference inputs. In physical system, inertial measurement unit, ultrasonic proximity sensor, and optical flow sensor have been used to measure state variables, Brushless DC motors and high-speed servo motors are used as actuators. After completion of the simulations, real-time system tests have been started. The control algorithm designed in MATLAB, Simulink. Real Time Windows Target has been used to implement real-time control via data acquisition board. In both simulations and real-time tests attitude and altitude have been successfully controlled.

Keywords: Tilt-rotor, trirotor, tricopter, Linear Quadratic Regulator, Altitude Control, Attitude Control, Real Time Windows Target, UAV

ÖZ

ÜÇ DÖNER ROTORLU İNSANSIZ HAVA ARACININ YÖNELİM VE İRTİFA DENETİMİ

Kaçar, Alp

Yüksek Lisans, Mekatronik Mühendisliği Bölümü

Tez Yöneticisi: Yrd. Doç. Dr. Kutluk Bilge Arıkan

Ortak Tez Yöneticisi: Yrd. Doç. Dr. Bülent İrfanoğlu

Temmuz 2013, - 53 sayfa

Bu tezde üç dönerkanatlı döner rotorlu bir insansız hava aracının (İHA) tasarımı ve İHA'nın yönelim ve irtifa dinamikleri için denetimci tasarımı çalışmaları yapılmıştır. Üç döner rotora sahip İHA isterlere gore tasarlandıktan sonra karbonfiber çubuklar, plastik parçalar, eğimlendirme mekanizması ve ayaklarının üretimi tamamlanmıştır. Tasarım sürecinde matematiksel model de kurulmuştur. Söz konusu model doğrusallaştırılmış, kararlılık ve referans girdi takibini sağlayacak doğrusal kuadratik regulator (LQR) tasarımı gerçekleştirilmiştir. Doğrusal ve doğrusal olmayan sistem için benzetim ortamında testler yapılarak, Q ve R matrislerinin son ayarlamaları yapılmıştır. Fiziksel sistemde; ataletsel ölçüm birimi, ultrasonik mesafe algılayıcı ve optik akış algılayıcıları kullanılmıştır. Fırçasız DC motorlar ve yüksek hızlı servo motorlar eyleyiciler olarak kullanılmıştır. Benzetimin tamamlanmasının ardından gerçek zamanlı donanım testleri başlamıştır. Denetim algoritması MATLAB, Simulink'te tasarlanmış olup; Real Time Windows Target ve veri toplama kartı kullanılarak gerçek zamanlı denetim uygulaması gerçekleştirilmiştir. Benzetim ve gerçek zamanlı test ortamında sistemin denetimi başarı ile sağlanmıştır.

Anahtar Kelimeler: Tilt-rotor, trirotor, trikopter, Doğrusal Kuadratik Regülator, İrtifa Denetimi, Yönelim Denetimi, Real Time Windows Target, İHA

To Humanity

ACKNOWLEDGEMENTS

I appreciate my supervisor Asst. Prof. Dr. Kutluk Bilge Arıkan for his guidance, support and patience. I would like to thank to my co-supervisor Asst. Prof. Dr. Bülent İrfanoğlu. Also, thanks to all of my co-workers in FİGES Engineering for their help and support, Kerem Başbuğ, Azizhan Tekin, Burak Pehlivanoğlu, Emre Güner and Fırat Tansu who always motivated me and are eager to assist me technically and mentally. Lastly, I would like to thank to Se Defense, and Ministry of Science, Industry and Technology for their financial support to 001134.STZ.2011-2 San-Tez Project and San-Tez Team Members Barışcan Tok, Ahmet Caner Kahvecioğlu, Onur Albostan, Onur Ünlü and Serkan Köse for their best affords.

TABLE OF CONTENTS

LIST OF TABLES

LIST OF FIGURES

LIST OF ABBREVIATIONS

3D	-	Three-Dimensional Space
A/D	-	Analog-to-Digital
ABS	-	Acrylonitrile Butadiene Styrene
AGL	-	Above Ground Level
AHRS	-	Attitude and Heading Reference System
ATU	-	Atılım University
BEC	-	Battery Eliminator Circuit
BLDC	-	Brushless Direct Current
CAD	-	Computer Aided Drawing
CG	-	Center of Gravity
DC	-	Direct Current
DoF	-	Degrees of Freedom
ESC	-	Electronic Speed Controller
FBD	-	Free Body Diagram
FRL	-	Flying Robotics Laboratory
GPS	-	Global Positioning System
I^2C	-	Inter-Integrated Circuit
IGBT	-	Insulated Gate Bipolar Transistor

IMU	-	Inertial Measurement Unit
INS	-	Inertial Navigation System
LED	-	Light Emitting Diode
Li-Po	-	Lithium - Ion Polymer
LQR	-	Linear Quadratic Regulator
MOSFET	-	Metal Oxide Semiconductor Field Effect Transistor
MSL	-	Mean Sea Level
OS	-	Operating System
PC	-	Personal Computer
PID	-	Proportional – Integral – Derivative
PCI	-	Peripheral Component Interconnect
PWM	-	Pulse Width Modulation
RC	-	Radio Control
RF	-	Radio Frequency
RT	-	Real Time
RTWT	-	Real Time Windows Target
SPI	-	Serial Peripheral Interface
UART	-	Universal Asynchronous Receiver/Transmitter
UAS	-	Unmanned Aerial System
UAV	-	Unmanned Aerial Vehicle
USB	-	Universal Serial Bus
V/STOL	-	Vertical and/or Short Take-Off and Landing
VTOL	-	Vertical Take Off and Landing

NOMENCLATURE

ϕ	-	Roll angle
$\dot{\phi}$	-	Roll angular rate
$\ddot{\phi}$	-	Roll angular acceleration
θ	-	Pitch angle
$\dot{\theta}$	-	Pitch angular rate
$\ddot{\theta}$	-	Pitch angular acceleration
Ψ	-	Yaw angle
$\dot{\Psi}$	-	Yaw angular rate
$\ddot{\Psi}$	-	Yaw angular acceleration
x_e	-	Linear displacement in x direction with respect to Earth Axis
$\dot{x_e}$	-	Linear velocity in x direction with respect to Earth Axis
$\ddot{x_e}$	-	Linear acceleration in x direction with respect to Earth Axis
y_e	-	Linear displacement in y direction with respect to Earth Axis
$\dot{y_e}$	-	Linear velocity in y direction with respect to Earth Axis
$\ddot{y_e}$	-	Linear acceleration in y direction with respect to Earth Axis
z_e	-	Linear displacement in z direction with respect to Earth Axis
$\dot{z_e}$	-	Linear velocity in z direction with respect to Earth Axis
$\ddot{z_e}$	-	Linear acceleration in z direction with respect to Earth Axis

m	-	Mass of the system
m_1	-	Mass of 1st rotor
m_2	-	Mass of 2nd rotor
m_3	-	Mass of 3rd rotor
I_{xx}	-	Moment of inertia of body in x axis
I_{yy}	-	Moment of inertia of body in y axis
I_{zz}	-	Moment of inertia of body in z axis
g	-	Gravitational acceleration
l	-	Length of body to center of gravity
F_{xb}	-	Force in body x direction
F_{yb}	-	Force in body y direction
F_{zb}	-	Force in body z direction
F_{xe}	-	Force in earth x direction
F_{ye}	-	Force in earth y direction
F_{ze}	-	Force in earth z direction
L	-	Moment around x direction
M	-	Moment around y direction
N	-	Moment around z direction
α_1	-	Angle of 1st Servo Motor
α_2	-	Angle of 2nd Servo Motor
α_3	-	Angle of 3rd Servo Motor
PWM_{ESC1}	-	PWM duty ratio of 1st ESC
PWM_{ESC2}	-	PWM duty ratio of 2nd ESC

PWM_{ESC3}	-	PWM duty ratio of 3rd ESC
PWM_{S1}	-	PWM duty ratio of 1st Servo Motor
PWM_{S2}	-	PWM duty ratio of 2nd Servo Motor
PWM_{S3}	-	PWM duty ratio of 3rd Servo Motor
c_i	-	Cosine of *i*
s_i	-	Sine of *i*

CHAPTER 1

INTRODUCTION

In the 21st century, Unmanned Aerial Vehicles (UAV) became a challenging research topic for researchers. Lots of different aerial vehicles are available today, and they are named generally according to number of rotors and/or structure. The aerial vehicles can divide into two main types, fixed wing aircrafts and rotary-wing aircrafts. Fixed-wing aircrafts are aircrafts capable of flight using wings that generate lift caused by the movement of the aircraft. There are two types of fixed-wing aircrafts; manned or unmanned. Airplanes, gliders and kites are examples of fixed-wing aircrafts. Rotary-wing aircrafts are capable of flight using the lift generated from rotor blades (rotary-wings). Helicopters, cyclocopters and other multi-rotor aircrafts are kind of rotary-wing aircrafts. Almost all rotary-wing aircrafts are capable of Vertical Take Off and Landing (VTOL) or Vertical and/or Short Take-Off and Landing (V/STOL). Multi-rotor aircrafts divides into several types according to their rotor numbers; single rotor, twin-rotor, tri-rotor (or tri-copter), quad-rotor (or quad-copter, quadrocopter), hexa-rotor (or hexa-copter) and so on [1]. Also, there is a special type of aircraft contains both fixed-wing and rotary-wing called tilt-rotor aircraft [2]. Manned fixed-wing and rotary-wing aircrafts are illustrated below in Figure 1.

Figure 1: Manned Fixed-wing Aircraft and Manned Rotary-wing Aircraft [3, 4]

In history, first UAV was developed by Charles Rozier in France for transporting bombs in 1818 [5]. UAV applications can be divided into two major areas such as: military operations and civil applications [1].

- Military Operations
  - Border Security
  - Security Intelligence
  - Coast Guard
  - Surveillance
  - Target Following

- Civil Applications
  - Search and Rescue
  - Pollution of Seas
  - Correction of Uncontrolled Trash Areas
  - Forest Fire
  - Illegal Urbanization
  - Control of Oil, Fuel and Connection Lines
  - Photography and Shooting Movie
  - Analysis of Fire Gas
  - Radiation Detection

Depending on the design approaches, researchers are tried to develop those structures become more efficient, more complex, and smaller, so that new concepts are added to the UAV portfolio. One of the new concepts is to reducing number of rotors and added actuators to the rotor to tilt this rotor to increase the maneuverability of the quad-rotors. The reduction in the number of rotors from four to three enables more compact vehicles (back packable UAVs) for rapid deployment, as well as longer flight autonomy.

1.1 Aim and Scope of Thesis

The aim of the thesis is to maintain attitude and altitude control of the designed triple tilt-rotor UAV. Thesis study is a part of a San-Tez Project (**001134.STZ.2011-2, Üç Dönerkanatlı Özerk Hava Taşıtı 3DÖHAT**). It is aimed to design a basic tri-copter platform with tilting rotors to be utilized in various UAV projects of the company – Se Defense (Se Savunma Sanayi Havacılık Elektrik Elektronik Mühendislik İmalat Sanayi Ticaret Ltd. Şti). Designed system has multiple operating modes and dynamical capabilities. It can be used as a fully-actuated system by using all of the six actuators or it can be used as an under-actuated system by using four or five of the available actuators (three propulsion units plus one or two tilting rotors). In this thesis complete actuator set is utilized during the controller design. Following items are covered in this thesis.

- **Mathematical modeling of the system is studied:** Dynamics of the propulsion units, namely the brushless dc motor and propeller is identified. Moment of inertia terms are also obtained experimentally.

- **Model based controllers are designed:** LQR based controllers are designed for both stabilization and reference tracking. Designed controllers are implemented in real-time by Real-Time Windows Target. Designed control systems are tuned during real-time implementations.

- **Attitude and altitude of the UAV is controlled:** Attitude and altitude control is achieved with linear state feedback control based on LQR design. Optical flow

sensing is studied. Use of optical flow in XY position control is left as a future work. Path tracking or target tracking is not covered.

1.2 Outline of the Thesis

In Chapter 2, the literature survey is discussed. Physical system is described in Chapter 3 with mechanical structure and components. Chapter 4, the mathematical model of the system is derived. The controller design and test results are mentioned in Chapter 5. Discussion and conclusion of thesis are stated in Chapter 6.

CHAPTER 2

LITERATURE SURVEY

Unmanned Aerial Systems (UAS) are studied in many various concepts. Systems with rotary wings and constant pitch angle propellers gained popularity in recent years. Mainly quad-copter with four rotary wing propulsion units is used as a standard platform due to their attractive properties and dynamical characteristics. In addition to this, research on twin-rotors, tri-rotors and other multi-rotor UAV is also done. The research on systems other than quad-rotors or quad-copters is motivated to reduce the number of actuators in the system or to improve the reliability of the system by increasing the number of propulsion units or to study under-actuated robotics, or to increase the payload and carrying capacity.

In this literature survey, work performance will be concentrated on first UAS work is a triple tilting rotor which is a novel design named Delta. The system has three rotors with tilting capability, but all tilting inputs of the system are the same. It is a mini UAV, which has the rotor to rotor distances as 0.3m and the weight of the system is 0.45Kg. For stabilizing the system, axial, lateral and longitudinal dynamics are separated. In this work low cost IMU and low cost embedded hardware are used. [6]

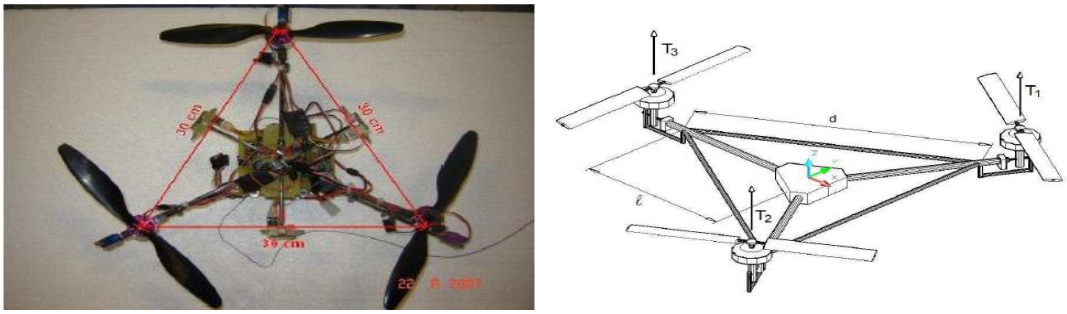

Figure 2: Delta Triple Tilting Rotor mini UAV [6]

In second work, different kinds of tri-rotor designs are analyzed. The similarities and differences between these designs are discussed. Coaxial, one tilted and without tilt rotor tri-rotors are worked. In that conceptual work one of the systems is a single tri-rotor (means tri-rotor with one tilting). When stabilizing a single tri-rotor, rapid motion from its tri-rotor could be a challenge because it requires a very accurate tilting angle for stabilizing of the system. One of the control strategies of the single tri-rotor is illustrated below. [7]

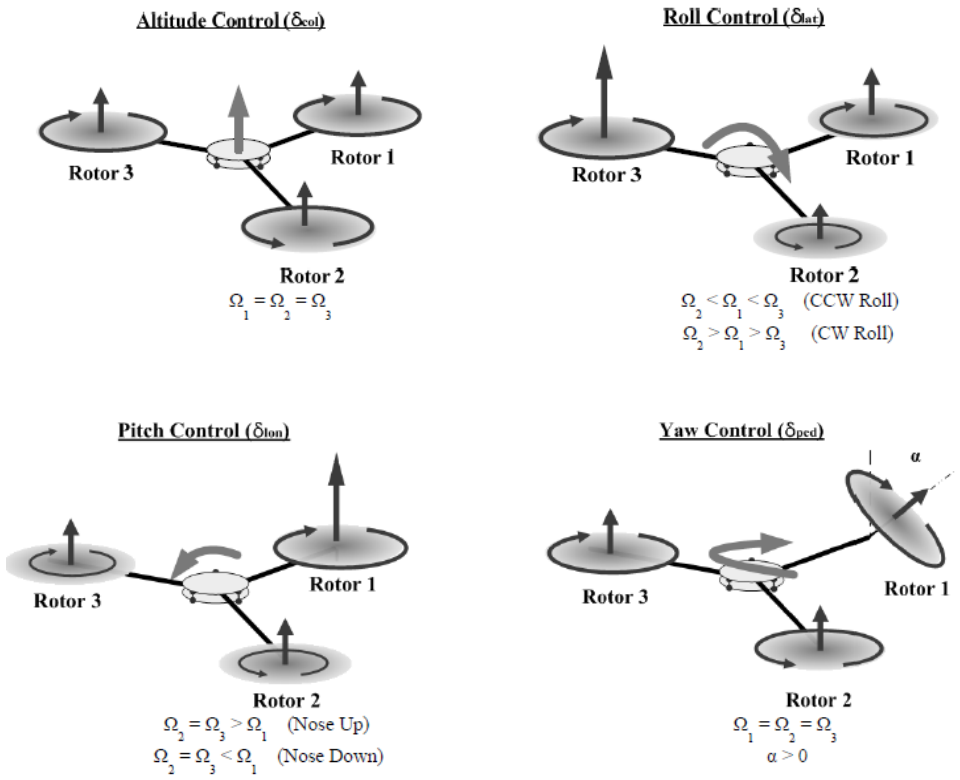

Figure 3: Altitude, Roll, Pitch and Yaw Control Strategies of a Single Tri-rotor [7]

In third work, a quad-rotor from DraganFly is modified. The forth bar and rotor are removed from the system and a tilting capability is added to one of the remaining rotors. The three-rotor vehicle is shown in Figure 4. It is equipped it with sensors, electronic circuits, motor drivers and microcontrollers, with xPC target OS is used for stabilization of the vehicle with Advantech PCL-726 and PCL818HG as data acquisition platform. Polhemus magnetic sensor is used for stabilization. [8, 9]

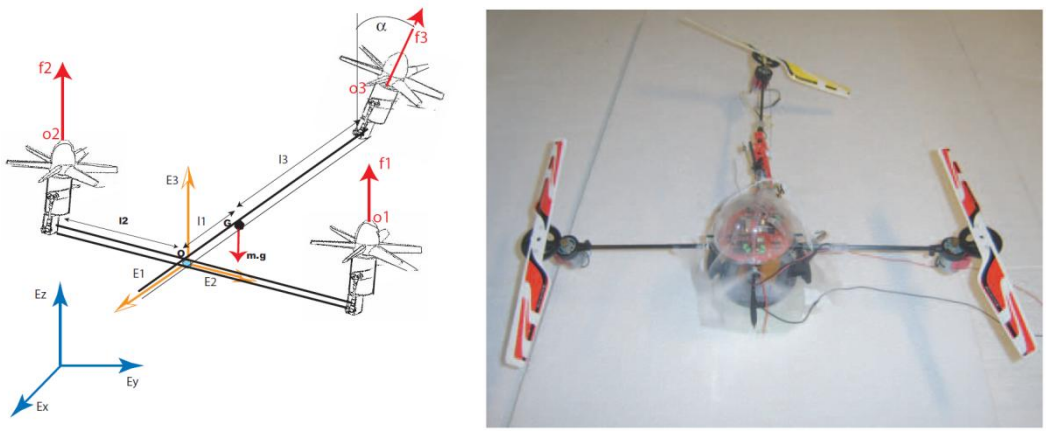

Figure 4: Modified DraganFly Tri-rotor with One Tilt [8]

The following 3 studies are done in Atılım University (ATU) in Mechatronics Engineering Department, Flying Robotics Laboratory (FRL). Toruk project is the first step of this thesis. In this project a novel twin-rotor UAV was designed. One of the rotors of the UAV has a tilting capability. DraganFly brushed type motor, Hi-tech wing servo motor is used as tilting motor, Microstrain 3DM-GX2 is used as IMU, and Humusoft MF614 is used for data acquisition hardware. Roll, pitch and yaw angles are controlled using a PID and decoupling control. MATLAB & Simulink with RTWT is used with 0.01s sample time. Also, there was a passive simple pendulum system attached to bottom side of the system. The mathematical model of the system derived using Newton-Euler formulation. The FBD and photo of the system is shown below. (Appendix A, [1, 2])

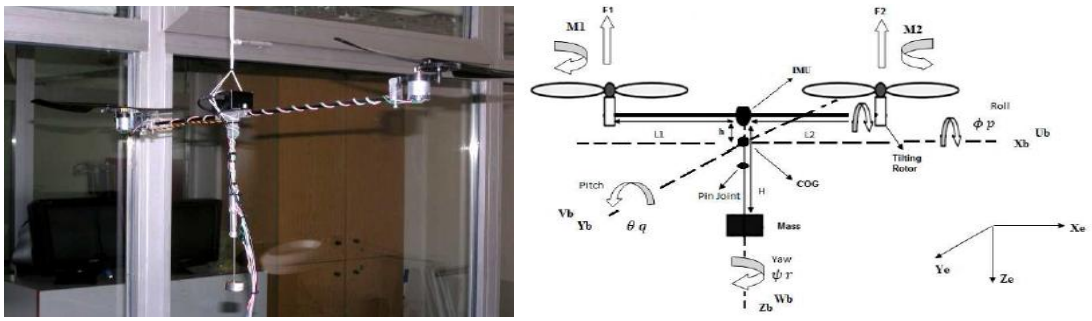

Figure 5: Toruk Project – Twin-rotor system with one tilting

One of the master theses from ATU is an outdoor quad-rotor platform. In the thesis, attitude and altitude dynamics are controlled using Simulink, xPC target. PID and LQR controller algorithms are used. During the implementation of the designed

controllers, different test setups are used. Humusoft MF624 is used as the DAQ card, four BLDC motors are used as propeller actuators, four ESCs as BLDC drivers, landing gears is used for safe landing, and Microstrain 3DM-GX3-25 IMU is used. Mathematical model of the quad-rotor is done first, then PID and LQR controllers are designed and implemented in MATLAB, Simulink environment. The controller adopted into real system and the parameters of the controllers are tuned. The photo of the system is shown in Figure 6. [1] In another master thesis from ATU. Attitude and altitude control of a hybrid wheel tri-rotor system is studied. The system has 2 wheels and 3 rotors and it can move on the ground or fly in the air. In this system, a control system is designed using LQR and feedback linearization. MATLAB & Simulink are used as the design and testing platform for the controllers. [10]

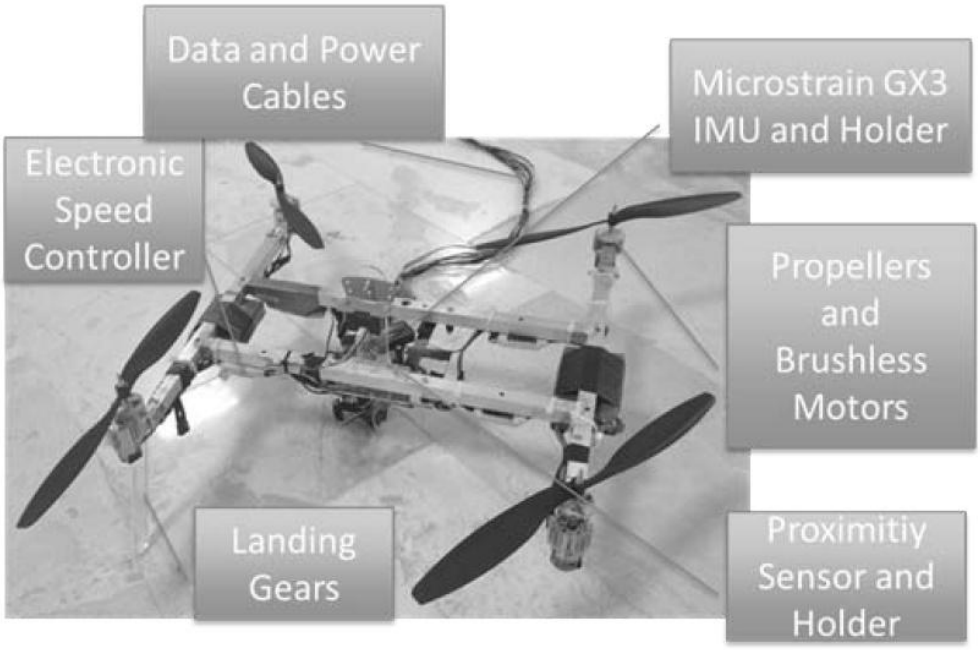

Figure 6: A Quad-rotor representation with its components [1]

Another tri-rotor study in literature includes the design and flight tests of a small tri-rotor UAV with LQR based attitude control system. This system also has a single tilt mechanism. Force and moment equations are derived and some unknown parameters of equations are calculated via experiments. LQR is applied for attitude control. Simulations are done for linearized and non-linear model. Attitude and heading reference system is used to sense the orientation. Overall system weight is

840g including the onboard controller with ATmega128 processor. Two bladed 7'propellers used with BLDC motors. Each motor is capable to generating 300g thrust. The sample time of the system is set to 0.01s and 50Hz PWM signals are generated used to drive ECSs. In Figure 7, the tilt mechanism and yaw control are shown. [11]

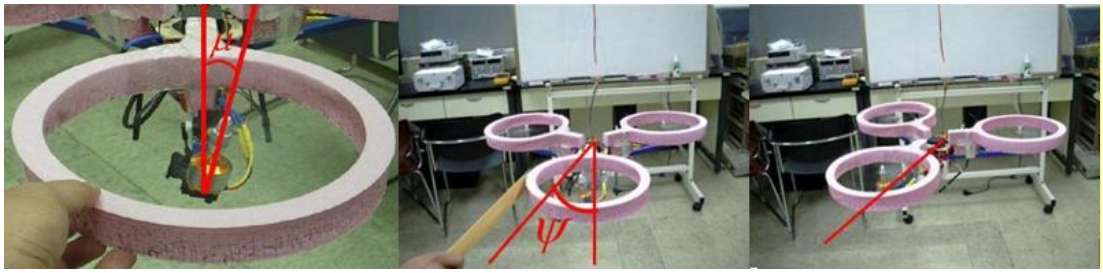

Figure 7: A Tri-rotor with one tilt mechanism [11]

Another work is Quad Tilting-Rotor UAV. Quad-rotors without tilting rotor capability are not capable of tracking an arbitrary trajectory over time. For instance, it can hover on the spot only when horizontal. In this work, four tilting rotors are attached to the system. This feature introduces an additional set of four control inputs which provides full actuation of position and orientation of the quad-rotor. In this work CAD model of the system is used in a 3D simulator. In the simulator, trajectory tracking controller based on dynamic feedback linearization is used for a parallelogram trajectory. The CAD model and trajectory tracking simulator figures are illustrated in Figure 8 below. [12]

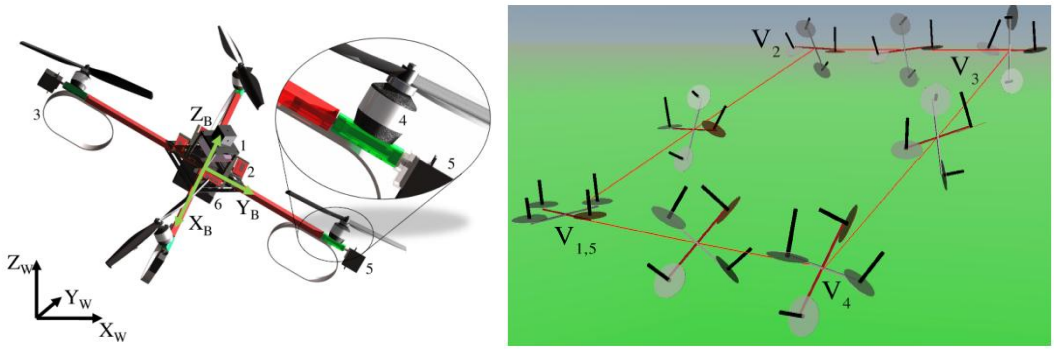

Figure 8: Quad-rotor with Tilting Rotors and Its Tracking Simulation [12]

An alternate tilt-rotor work is a twin-rotor system with double axis tilting. In this work each rotor has both lateral and longitudinal tilting capability. The aim of the

project is to reduce the number of the rotors. The pitch stability is increased by combining the opposed lateral tilting with the longitudinal tilting of two rotors. The paper says *"A theoretical analysis of this mechanism proves its effectiveness and the experimental results show that this aerodynamical configuration is very promising."* In the Figure 9 below, photos of the system is illustrated. [13]

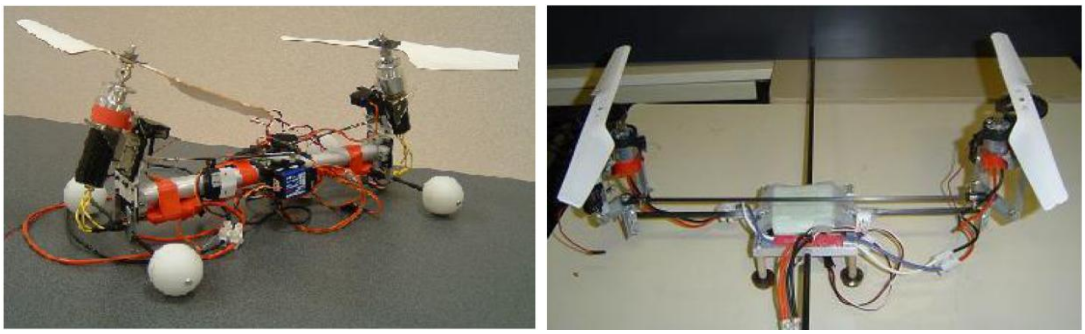

Figure 9: A Twin-rotor System with Lateral and Longitudinal Tilting Rotors [13]

Another study is a Master of Science thesis from Cornell University. It includes structural and control improvements in the design of the X4-flyer quad-rotor and its controller. The X4-flyer quad-rotor is originally a non-tilt-rotored quad-rotor. In the thesis, brushed type hobby motors are utilized as rotors, APC propellers, and Li-Po batteries are used also. Both PID and LQR controllers are used for stabilization. For finite element model ANSYS, for dynamical model MATLAB and for controller design and simulation Simulink are used as software platforms. The reference control input given to the system is supplied by human input via RC. The CAD model and photo of the system is given below in Figure 10. [14]

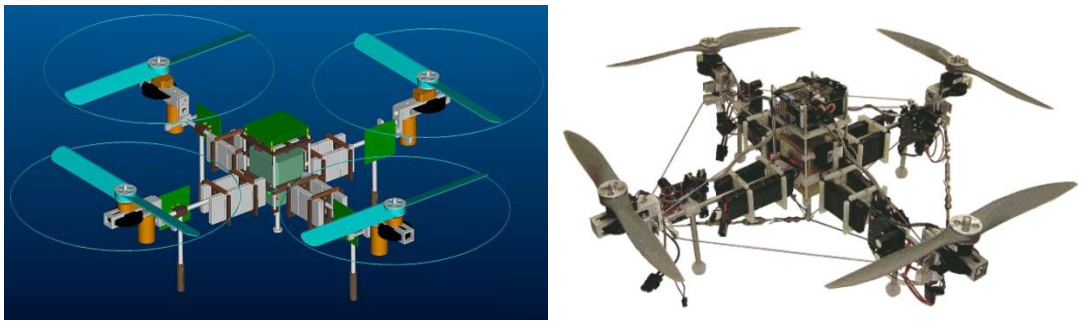

Figure 10: Improved X4-flyer Quad-rotor [14]

The final work of the literature survey is the design and control of an autonomous quad-rotor UAV named OS4. DSP controller and 266MHz Geode 1200 processor are used as embedded controllers. For obstacle avoidance and altitude detection ultrasonic sensors are used with I^2C interface. Wireless network adapter is used for control data and programming. Bluetooth received and transmitter is used for reference input and a video transmitter and receiver are used for getting video from the UAV. Also, low-cost IMU, motors and its drivers, and Li-Po batteries are used. PID, LQ, adaptive optimal controller, back-stepping, sliding-mode, integral back-stepping (with augmented states) controller algorithms are used for stabilizing the system. The test steps of the system are illustrated in Figure 11 below. From left to right, first figure represents test-bench with an universal joint, second is photo of the miniature of the system, third one is last version of the OS4 and last one is flight test. [15]

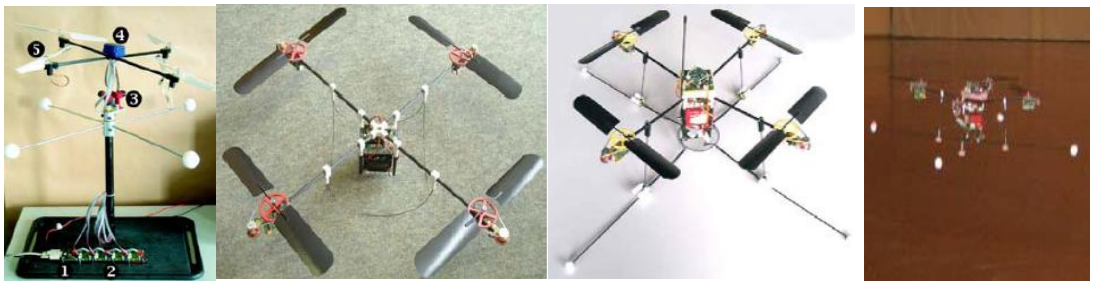

Figure 11: OS4 Quad-rotor [15]

In the literature survey part, tilting twin-rotors, tri-rotors and quad-rotors and non-tilting UAVs are summarized. According to these works, this thesis is taken its shape. Some applications of these works are planned to be improved and adapted to the triple tilt-rotor UAV system. There is not a triple tilt-rotor platform that uses different tilt actuation signals. Also, almost none of the studies prove the rigidness of the system.

CHAPTER 3

PHYSICAL SYSTEM

In this thesis, a fully-actuated tri-rotor platform is designed. The physical system has structural components, sensors, actuators, control hardware and software. Main structure or the chassis is designed by San-Tez Project team by performing required analysis and optimizations using finite element method. In parallel with these finite element analyses, mathematical models for guidance and navigation are designed. These two modeling architectures are utilized in parallel throughout the project. Component selection is also based on these models. System integration is performed after the relevant tests of individual subsystems. Figure 12 presents the simplified schematics of the system with basic components and their interrelations.

Two Humusoft MF624 Data Acquisition Cards are utilized for real-time control and data acquisition purposes. Also, Microstrain GX3 Inertial Measurement Unit is utilized via RS-232 protocol.

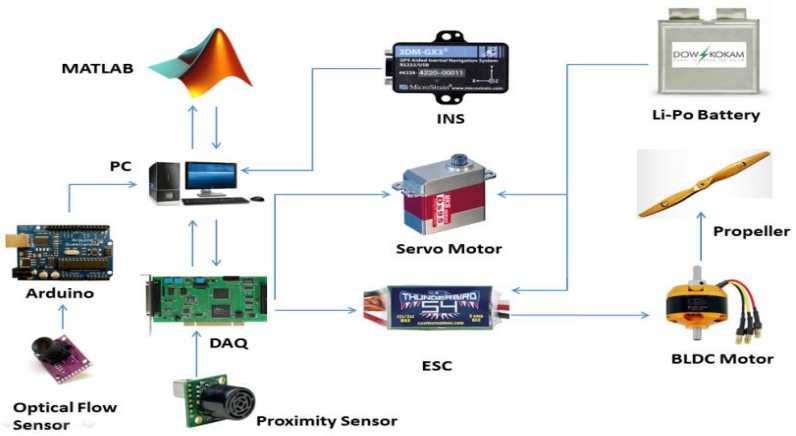

Figure 12: Physical System Schematics

High speed MKS DS95 Servo motors are used in the tilting mechanism. They receive position reference inputs with 333Hz PWM signal via one of the Humusoft MF624 DAQ board. Brushless motors, Scorpion, in propulsion units are driven by Thunderbird 54 drivers (namely electronic speed controllers, ESC) with 300Hz PWM signal via the other MF624 board. Ultrasonic proximity sensor is connected to A/D port of MF624. Optical flow sensor, Avago ADNS-3080, is used to sense the translational deviation in XY plane. A microcontroller Arduino Duemilanove is used to receive optical flow sensor output and send to main controller.

3.1 Mechanical Structure

Three different types of chassis have been used in literature: Y-shaped chassis [7], T-shaped chassis [8] and delta shaped chassis [6]. In this project, Y-shaped chassis in Figure 14 is preferred due to the structural properties, ease of manufacturing, practical aspects for the optimum design, etc. Structural vibration analysis is also performed using finite element analyses. 1/3 of the system is taken for doing finite element analyses (from right to left, first figure). After the beam is prepared as a finite element model, 1st, 2nd, and 3rd modal analyses are done in ANSYS as shown in Figure 13 (from right to left respectively).

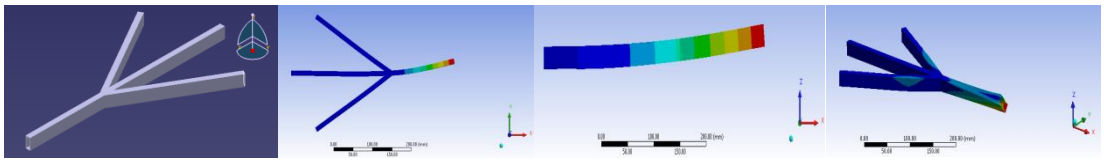

Figure 13: Beam Design and 1, 2, and 3. Modal Analyses Results

Using finite element analyses, deformations on chassis are decreased and in the simulations the body is taken as rigid body. These analyses are done with contributions of the San-Tez team.

Design should consider the aspects related to structural vibration. Sensor set, actuators and related electronics are all affected from vibration in addition to the structural rigidity. According to the analysis, stiffener beams are included in the design to reduce the structural vibrations and improve the strength.

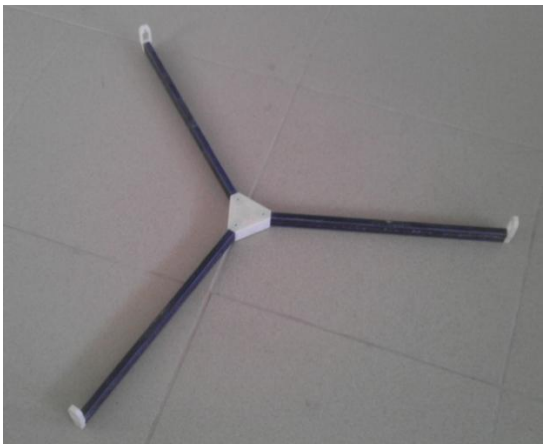

Figure 14: Y-chassis (First Step of Prototype)

This is the combination of the Y and delta chassis types. As shown in Figure 15 below, six similar carbon fiber (CF) bars are attached with ABS parts and tilting mechanism. (Appendix A, [2])

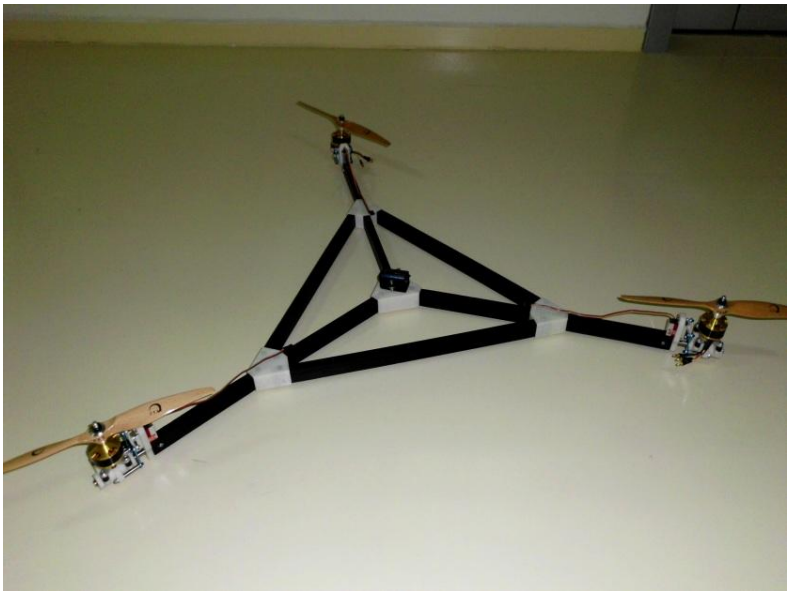

Figure 15: Assembled Prototype

Rotor to rotor distance of the system is 0.8 m and CF bars' length is 0.55 m. System has landing gears with 0.2 m of height. In appendix B overall system assembly and tilt mechanism drafts are attached. The weights of the subsystems are shown below in Table 1.

Table 1: Weight of the subsystems

Part Name	**Quantity**	**Unit Weight (g)**	**Total Weight (g)**
Carbon Fiber Bar	6	45	270
Main Connector	2	19	38
Stiffener Connector	6	10	60
Landing Gear	3	11	33
Tilt Mechanism	3	140	420
INS	1	19	19
ESC	3	34	102
BLDC Motor + Prop.	3	120	360
Miscellaneous	1	140	140
Total System Weight			1442

One of the major constraints in the design is related with the weight and total maximum thrust of the propulsion units. Total weight including the payload should not exceed 60% of the total maximum thrust [16, 17]. Also, landing gears have a height of 20cm. To handle ground effect, the propellers must have a height of radius of propellers [18]. Overall design satisfies this major constraint. Part of design procedure of the complete system worked with San-Tez team is not given in details in the thesis. It is an iterative process which is carried on between mathematical model and design criteria. All the details of the design of the system are not given in the thesis, since it is performed with San-Tez Team (Appendix A, [2, 3, 4]).

3.1.1 Carbon-Fiber (CF) Bars

Carbon-fiber bars were manufactured in Se Defense with the contributions of the San-Tez team. Within the process, there are several steps to be considered. Before initiating the processes, the aluminum mold of the bar was designed, manufactured and mold release liquids rolled onto it 4-5 times. Firstly, a balsa bar, CF fabrics, and protection nylons were cut to proper sizes. CF fabrics wrapped over balsa via adding epoxy and resin combination. After the rolling operation, a fiberglass layer rolled onto it also. The part is laid on to bottom mold and top mold was closed on it. The CF bar manufacturing process completed after 2 hours waiting in 40 ^{o}C oven. In Figure 16 balsa bar, epoxy and resin, bottom and top molds, and completed CF bar are shown respectively [19].

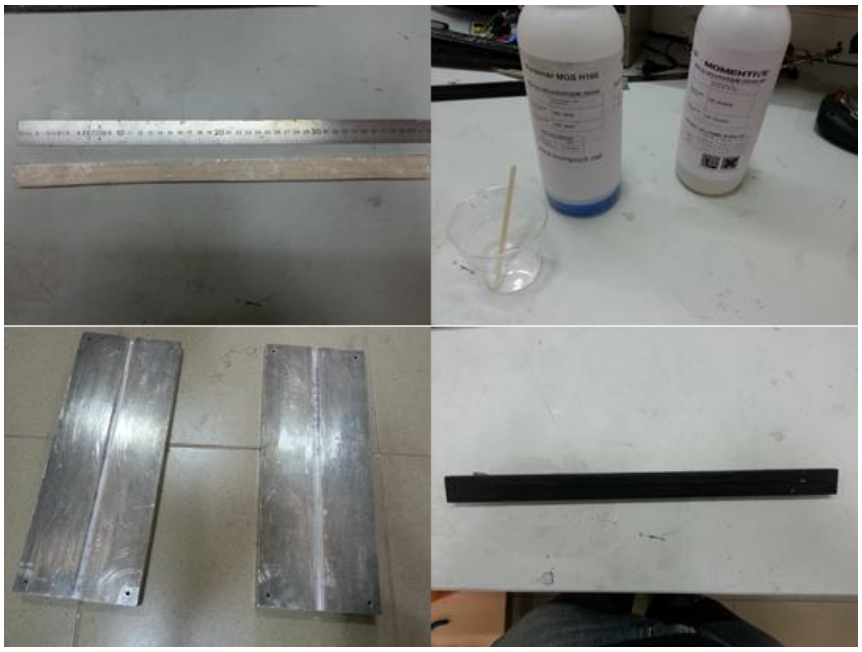

Figure 16: CF Manufacturing Processes

3.1.2 ABS

ABS (Acrylonitrile Butadiene Styrene) parts are designed by San-Tez Team via CATIA V5 and manufactured in ATU laboratories using Stratasys Fortus 400MC 3D prototyping machine with ABS-M30 material. 2 pieces of main connector, 6 pieces stiffener connector, 3 pieces for Servo motor holders, and 3 pieces for tilting mechanism are manufactured.

3.1.3 Tilt Mechanism

All tri-rotor UAVs must have a tilt mechanism to control the yaw dynamics. In the literature, there are exists several tilting mechanisms. These examples from literature and RC models are shown in Figure 17.

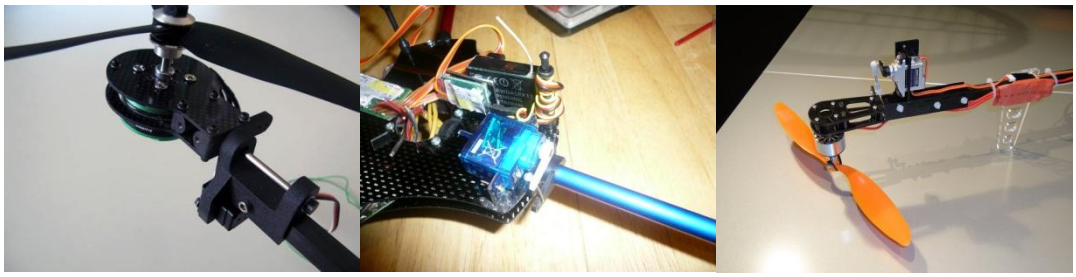

Figure 17: Example Tilt Mechanisms [20, 21, 22]

Most of the tilting mechanisms are direct drive. In direct drive mechanisms the weight of the motor-propeller and the force due to thrust act on the shaft of tilt actuation. That could cause problems in the motor, so parallelogram mechanisms are better solutions especially for heavy systems. After the type of the mechanism is chosen as a parallelogram, the axial load is calculated. Considering this axial load main shaft, lateral shafts, ball bearings, and tilt servo motor are selected. The lateral shafts have a diameter of 6 mm and main shafts have of 8 mm. Ball bearings selected as SKF W-628-8-2Z. There are 4 anti-vibration bolts between out-runner motor and tilt mechanism. The tilt mechanism is illustrated below in Figure 18.

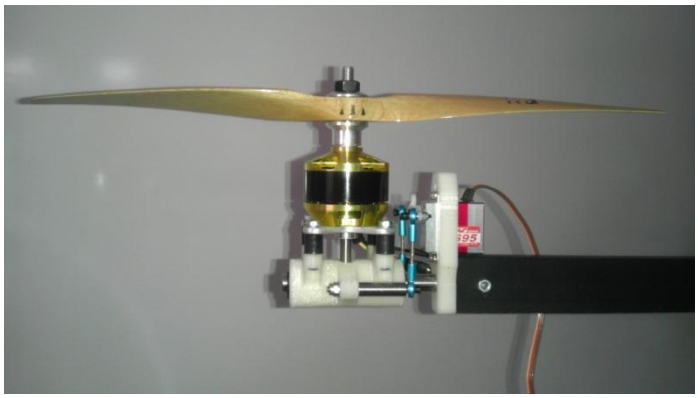

Figure 18: Tilt Mechanism

3.2 Servo Motor

The torque needed in the tilt mechanism is calculated according to the requirements of thrust. It is found as 0.02 kg.m of torque is needed. In addition to torque requirements, the servo motor should give fast response to maintain the stability of the closed loop system and performance. The frequency of the control loop is 300 Hz. Servo motor should also have an appropriate control frequency. PWM carriage frequency can be set up to 333Hz for MKS DS95. The duty cycle of the PWM is 27% to 72% to generate 1ms to 2ms duty ratio. The properties of MKS DS95 are illustrated in Table 2 and photo of it is shown in Figure 19 below.

Table 2: Properties of MKS DS95 Servo Motor

Dead band:	0.001ms
Control System:	Pulse Width Control (+)
Working frequency:	1500µs / 333Hz
Data:	850µs~2150µs

(RX) Required Pulse:	3.0~5.0 Volt Peak to Peak Square Wave
Operating Voltage:	4.8~6.0V DC
Operating Temperature Range:	-10 to + 60 Degree C
Operating Speed (4.8V):	0.066 sec/60° degrees at no load
Operating Speed (6V):	0.053 sec/60° degrees at no load
Stall Torque (4.8V):	2.44 kg.cm
Stall Torque (6V):	3.05 kg.cm
Connector Wire Length:	20.0cm
Dimensions:	23x12x27.25mm
Weight:	21.21g

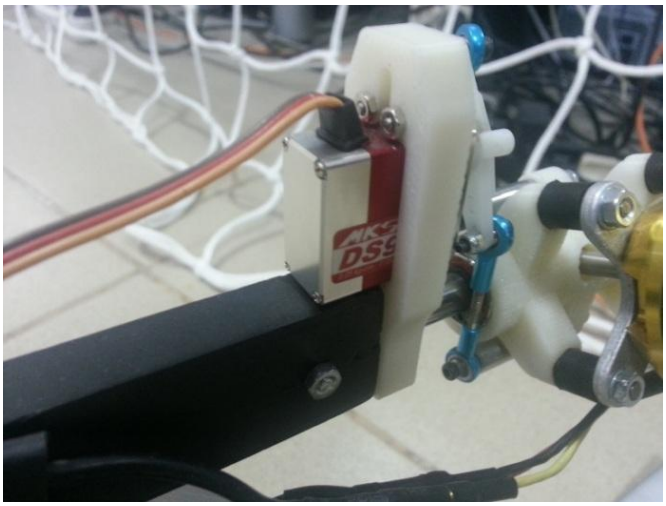

Figure 19: MKS DS95 Servo Motor

3.3 Brushless DC Motor

As indicated before total weight of the system is less than the 60% of the total maximum thrust. The rest is used for control purposes. The thrust is calculated with different propellers via Scorpion Calculator which belong to Scorpion System Motors. Considering the desired flight duration and payload, power requirement is calculated and 1.3 kg Li-Po battery is found to be the most appropriate one. This selection sets the requirement of 4.5 kg force total thrust, so 1.5 kg force of thrust is needed for a single propulsion unit. The rotor's BLDC motor is Scorpion Systems SII 3008 1220KV and the propeller is APC 11x5.5 E. The properties of Scorpion BLDC motor are shown in Table 3 and Figure 20 with the current configuration, the design could reach a flight time of 20 minutes.

Table 3: Properties of Scorpion BLDC Motor

Stator Diameter	30.0 mm
Stator Thickness	8.0 mm
No. of Stator Arms	12
Magnet Poles	14
Motor Kv	1220 RPM/Volt
No-Load Current (IO/10V)	0.97 Amps
Motor Resistance (Rm)	0.042 Ohms
Max Continuous Current	32 Amps
Max Continuous Power	425 Watts
Weight	95 Grams
Outside Diameter	37.50 mm
Shaft Diameter	4.98 mm
Body Length	33.75 mm
Overall Shaft Length	62.5 mm
Max Li-Po Cell	4S - 16.8V
Motor Timing	5deg
Drive Frequency	8kHz

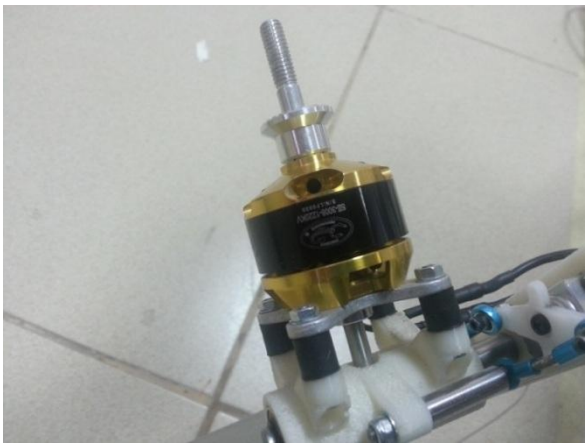

Figure 20: Scorpion Systems SII 3008 1220KV BLDC Motor

3.4 ESC

ESC is an electronic speed controller for brushless DC motors, in other words it is a BLDC motor driver. It contains 6 sets of MOSFETs or IGBTs for amplifying PWM signals, generated by a microcontroller. The motor used in this thesis, requires o a continuous current of 32A.

Table 4: Properties of Thunderbird 54 ESC

Max Amps:	54
Max Volts:	15 volts 3S Lipo
BEC:	Linear regulator 3 Amp Max.
Length:	50.8mm
Width:	29.2mm
Height:	10.16mm
Weight:	34g
Brake:	On/Off

Thunderbird ESC can be driven with up to 300Hz, between 30% and 60% duty cycle and it has 3 ampere BEC besides 54A driving current. The specifications of the ESC are shown above in table 4 and the Figure 21.

Figure 21: Thunderbird 54 ESC

3.5 Propeller

11 x 5.5 APC Thin Electric propeller is used. This propeller is selected using Scorpion Systems Software. ESC, BLDC motor and propeller are tested in a thrust measurement system as shown in Figure 22. In the thrust measurement setup, weighting scale is used for sensing of the thrust in terms of g.f (gram force) with a seesaw mechanism.

Figure 22: Thrust Measurement System

In the thrust measurement experiment, a PWM signal is sent to ESC to drive BLDC motor with APC propeller. Servo driver generates 300Hz PWM signal, which has a duty ratio between 30% and 60% (1ms and 2ms). The plot shown in Figure 23 is obtained by varying the PWM signal and recording to thrust values [23].

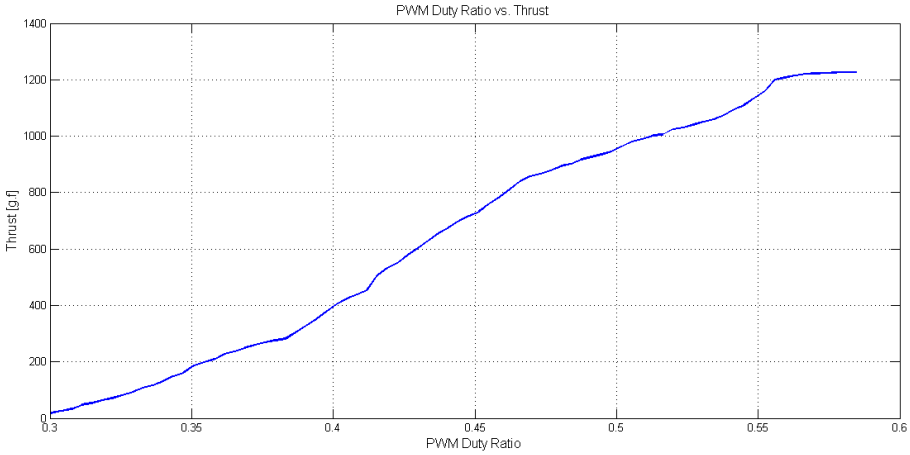

Figure 23: PWM to Thrust Graph

3.6 Sensor Set

Sensor set used on the system includes an Inertial Measurement Unit, IMU, a proximity sensor to measure the altitude, and the optical flow sensor to measure the deviation on XY plane, i.e. ground. Optical flow sensor can also be used to estimate the translational velocity.

Microstrain 3DM-GX3 IMU is selected as the inertial sensor that is shown in Figure 24. It has three different models; IMU - AHRS (-25), GPS aided AHRS (-35), and INS (-45). 3DM-GX3 Inertial sensor includes three axis accelerometer, gyroscope, magnetometer, temperature sensor and GPS. [24]

Figure 24: Microstrain 3DM-GX3 ®

For detecting the altitude, Maxbotix EZ3 – MB1230 ultrasonic proximity sensor is used as seen in Figure 25. This sensor is capable of reading distance between 0.200 m to 0.765 m and it can send the data up to10 Hz. MB1230 has 3 different data output mode; UART, PWM and analog voltage output. Analog output is used as output.

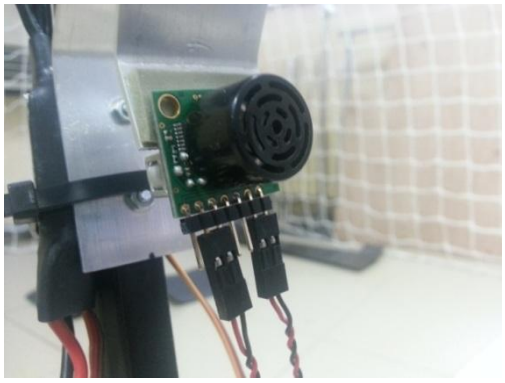

Figure 25: Ultrasonic Proximity Sensor

For sensing the distance travelled in X and Y directions, Avago ADNS-3080 optical flow sensor is utilized in the thesis. The sensor is shown in Figure 26. Fusion of the inertial measurement unit and optical flow sensor by Kalman filter, particle filter etc. are not covered in this study. Output of the sensor is monitored after a basic low-pass filter. Only the altitude measurement is required in the related Equation 3.1.

Figure 26: Avago ADNS-3080 Optical Flow Sensor

The sensor has a SPI interface for communication. Since RTWT cannot use SPI, there is a need for converting SPI to UART. The SPI to UART conversion is done using Arduino Duemilanove. Arduino is connected to PC via USB. The sensor sends change in X (delta X) and change in Y (delta Y). Delta X and delta Y are the data of the differences in movement between the previous and current position. According to the altitude of the sensor the delta X and delta Y are changed. The distance moved is calculated using the equation below. [25]

$$distance\ rate = \left(\frac{sensor\ value\ x\ altitude}{resolution\ x\ scalar}\right)\ x\ 2\ x\ tan\left(\frac{field\ of\ view}{2}\right) \qquad (3.1)$$

The sensor's resolution is default 400 pixels, the field of view is 12.62 degrees, and the scalar value is 1.

CHAPTER 4

MATHEMATICAL MODELLING

4.1 Dynamical Model

The mathematical model of the triple tilt rotor UAV is derived via Newton-Euler Method under certain assumptions [26]. In the Figure 27, final design of the triple tilt-rotor UAV is shown.

Figure 27: Triple Tilt-rotor UAV

Firstly, force and moment equations are derived with an assumption that UAV does not tilt its rotors. Then, tilting forces are calculated [27]. All parts of the system are taken as a rigid-body. The following equations show how mathematical model is derived.

The fixed reference frame is defined(x_e, y_e, z_e) as shown in Figure 28:

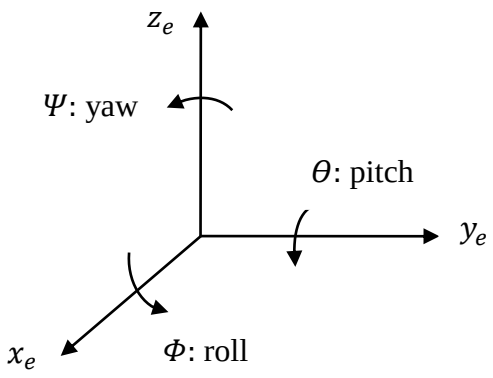

Figure 28: Earth Reference Frame

After the fixed frame is defined, transformation equations to body-fixed reference frame is defined as; [26]

$$\Psi \text{ Rotation: } R_1 = \begin{bmatrix} x_1 \\ y_1 \\ z_1 \end{bmatrix} = \begin{bmatrix} c_\psi & s_\psi & 0 \\ -s_\psi & c_\psi & 0 \\ 0 & 0 & 1 \end{bmatrix} \text{ (rotation about z axis)} \quad (4.1)$$

$$\theta \text{ Rotation: } R_2 = \begin{bmatrix} x_2 \\ y_2 \\ z_2 \end{bmatrix} = \begin{bmatrix} c_\theta & 0 & -s_\theta \\ 0 & 1 & 0 \\ s_\theta & 0 & c_\theta \end{bmatrix} \text{ (rotation about y axis)} \quad (4.2)$$

$$\Phi \text{ Rotation: } R_3 = \begin{bmatrix} x_3 \\ y_3 \\ z_3 \end{bmatrix} = \begin{bmatrix} 1 & 0 & 0 \\ 0 & c_\phi & s_\theta \\ 0 & -s_\theta & c_\phi \end{bmatrix} \text{ (rotation about x axis)} \quad (4.3)$$

Multiplication of the rotation matrices is shown in Equation 4.4 and 4.5. [26]

$$R_3 = \begin{bmatrix} x_3 \\ y_3 \\ z_3 \end{bmatrix} = \begin{bmatrix} 1 & 0 & 0 \\ 0 & c_\phi & s_\theta \\ 0 & -s_\theta & c_\phi \end{bmatrix} . \begin{bmatrix} c_\theta & 0 & -s_\theta \\ 0 & 1 & 0 \\ s_\theta & 0 & c_\theta \end{bmatrix} . \begin{bmatrix} c_\psi & s_\psi & 0 \\ -s_\psi & c_\psi & 0 \\ 0 & 0 & 1 \end{bmatrix} \quad (4.4)$$

$$R = \begin{bmatrix} -c\theta c\psi & c\psi s\theta s\phi & s\phi s\psi + c\phi c\psi s\theta \\ c\theta s\psi & c\phi c\psi + s\theta s\phi s\psi & \text{c}\phi\text{s}\theta\text{s}\psi - \text{c}\psi\text{s}\phi \\ -\text{s}\theta & \text{c}\theta\text{s}\phi & \text{c}\theta\text{c}\phi \end{bmatrix} \quad (4.5)$$

Transformation matrix has following properties:

$$\left(R^T\right)^{-1} = R \Leftrightarrow R^T = R^{-1} \tag{4.6}$$

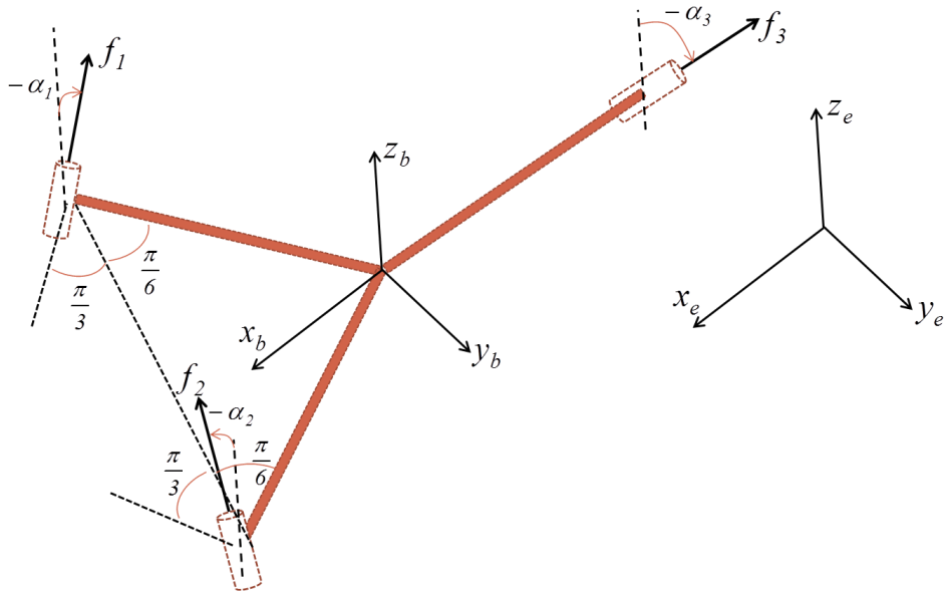

Figure 29: Isometric Schematic with Axes Representation

The inertia matrix is expressed as follows;

$$I = \begin{bmatrix} I_{xx} & -I_{xy} & -I_{xz} \\ -I_{yx} & I_{yy} & -I_{yx} \\ -I_{zx} & -I_{zy} & I_{zz} \end{bmatrix} \tag{4.7}$$

If off-diagonal elements of inertia matrix are negligible (theoretically they should be 0, but according to CAD model they are very small), they could be assumed to be 0 [28]. Lagrange equations are used to derive the equations of motion for rotational dynamics [6-8]. Following equations present the second time derivative of Euler angles:

$$\ddot{\theta} = \dot{\psi}\dot{\phi}(I_{YY} - I_{ZZ}) / I_{XX} + L / I_{XX} \tag{4.8}$$

$$\ddot{\phi} = \dot{\theta}\dot{\psi}(I_{ZZ} - I_{XX}) / I_{YY} + M / I_{YY} \tag{4.9}$$

$$\ddot{\psi} = \dot{\phi}\dot{\theta}(I_{XX} - I_{YY}) / I_{ZZ} + N / I_{ZZ} \tag{4.10}$$

Force equations obtained by Newton's 2nd law of motion. F_{xb}, F_{yb} and F_{zb} represent the components of resultant force vector in the body-fixed reference frame. (Appendix A, [3])

$$F_b = \begin{bmatrix} F_{xb} \\ F_{yb} \\ F_{zb} \end{bmatrix} = m.a_b \tag{4.11}$$

Using Equation 4.5, F_{xe}, F_{ye} and F_{ze} are obtained as;

$$\begin{bmatrix} F_{xe} \\ F_{ye} \\ F_{ze} \end{bmatrix} = R \times \begin{bmatrix} F_{xb} \\ F_{yb} \\ F_{zb} \end{bmatrix} \tag{4.12}$$

From the Equation 4.12, Equation 4.13, 4.14 and 4.15 are obtained as;

$$\ddot{x}_e = F_{xe} / m \tag{4.13}$$

$$\ddot{y}_e = F_{ye} / m \tag{4.14}$$

$$\ddot{z}_e = F_{ze} / m \tag{4.15}$$

According to sine and cosine components of f_1, f_2, f_3 and τ_1, τ_2, τ_3 on body x_b-y_b plane are shown on Figure 30 below.

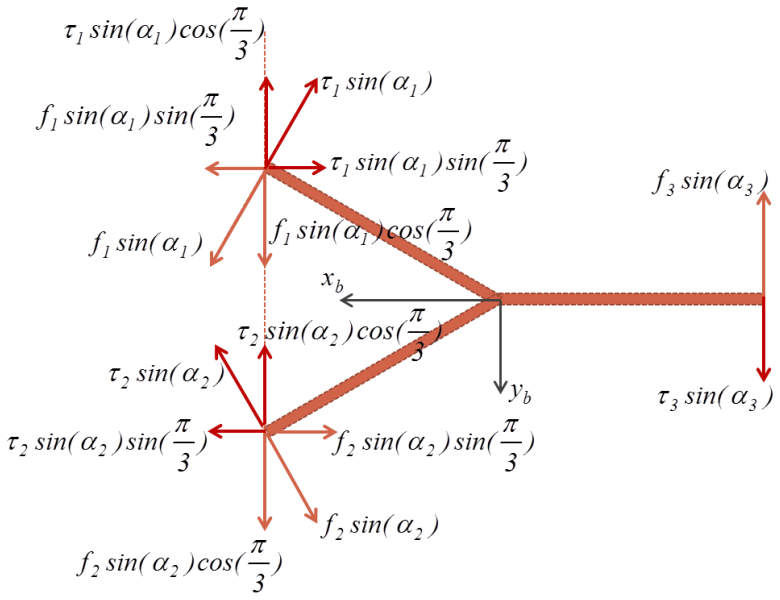

Figure 30: Forces and Moments on Body x_b-y_b Plane

The tilting mechanisms' sine and cosine components of f_1 and τ_1 are shown below on Figure 31. For other two axes it is same.

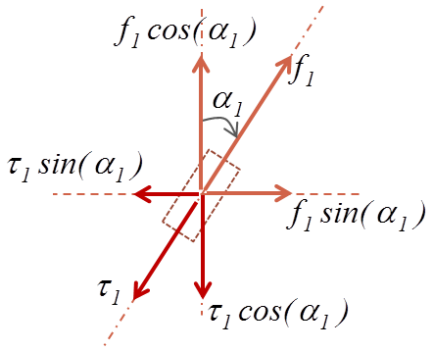

Figure 31: Force and Moment Components

Acting forces on the body in terms of thrust generated from the BLDC motors f_1, f_2, f_3 and tilt angles α_1, α_2, α_3 are shown below in Equations 4.16, 4.17, and 4.18.

$$F_{xb} = f_1 \sin(\alpha_1)\sin(\frac{\pi}{3}) - f_2 \sin(\alpha_2)\sin(\frac{\pi}{3}) + mg\sin(\theta) \quad (4.16)$$

$$F_{yb} = f_1 \sin(\alpha_1)\cos(\frac{\pi}{3}) + f_2 \sin(\alpha_2)\cos(\frac{\pi}{3}) - f_3 \sin(\alpha_3) - mg\cos(\theta)\sin(\phi) \quad (4.17)$$

$$F_{zb} = f_1 \cos(\alpha_1) + f_2 \cos(\alpha_2) + f_3 \cos(\alpha_3) - mg\cos(\phi)\cos(\theta) \quad (4.18)$$

Using the same approach with the force equations, moments equations are obtained as shown below in Equations 4.19, 4.20, and 4.21.

$$L = [f_2 \cos(\alpha_2) - f_1 \cos(\alpha_1)]l\cos(\frac{\pi}{6}) + [\tau_2 \sin(\alpha_2) - \tau_1 \sin(\alpha_1)]\sin(\frac{\pi}{3}) \quad (4.19)$$

$$M = -[f_1 \cos(\alpha_1) + f_2 \cos(\alpha_2)]l\sin(\frac{\pi}{6}) + f_3 \cos(\alpha_3)l - \left[\tau_1 \sin(\alpha_1)\cos(\frac{\pi}{3}) + \tau_2 \sin(\alpha_2)\cos(\frac{\pi}{3}) - \tau_3 \sin(\alpha_3)\right] \quad (4.20)$$

$$N = -[\tau_1 \cos(\alpha_1) + \tau_2 \cos(\alpha_2) + \tau_3 \cos(\alpha_3)] + [f_1 \sin(\alpha_1) + f_2 \sin(\alpha_2) + f_3 \sin(\alpha_3)]l \quad (4.21)$$

After the force and moment equations desired, the equations between ESCs' PWM signals and thrusts, and the equations between Servos' and tilt angles are obtained. The following equations are calculated using PWM to thrust ratio.

$$PWM_{ESCi} = 0.3 + \frac{0.3F_i}{1.225g}, \text{ where } i = 1, 2, 3 \quad (4.22)$$

$$PWM_{Si} = 0.27 + 0.45\frac{\alpha_i + \pi/4}{\pi/2}, \text{ where } i = 1, 2, 3 \quad (4.23)$$

In the equations derived, all states and inputs are defined. The system is a 6 DoF system and it has 6 independent actuator inputs ($PWM_{ESC1}, PWM_{ESC2}, PWM_{ESC3}$, $PWM_{S1}, PWM_{S2}, PWM_{S3}$), showing that the system is a fully actuated system [29]. To validate this assumption; consider the generalized coordinate vector *q* below.

$$q = \begin{bmatrix} \theta & \phi & \psi & x_e & y_e & z_e \end{bmatrix}^T \quad (4.24)$$

Second time derivative of the generalized coordinate vector is written as below.

$$\ddot{q} = f(q,\dot{q}) + g(q,\dot{q},u) \quad (4.25)$$

Where *u* is the input vector including the duty ratios of brushless motors and servo motors. It is seen that the system is non-affine in inputs. Therefore, jacobian matrix of vector $\underline{g}$ with respect to the input vector, *u*, is analyzed to present the fully-actuated characteristics of 3DöHaT. Jacobian matrix has a full rank of 6 (dimension of q vector is 6x1) revealing the fully-actuation characteristics locally. In fact, the determinant of the jacobian matrix is nonzero (indication of a rank less than 6) unless none of the thrusts generated by the propulsion units is zero. Zero thrust condition is not possible for our system. Therefore, we have concluded that fully-actuated condition is valid globally.

CHAPTER 5

CONTROLER DESIGN AND TESTS

Linearized model is used to design linear LQR based controllers. Utilized control system is previously applied on the attitude and altitude control of quad-rotors in Flying Robotics Laboratory at Atılım University. Successful results are obtained on quad-rotors. Normalized version of the LQR design is utilized in this thesis.

5.1 Linearization

State vector, *x*, is given below.

$$x = \begin{bmatrix} \theta \\ \phi \\ \psi \\ \dot{\theta} \\ \dot{\phi} \\ \dot{\psi} \\ \dot{z}_e \\ z_e \end{bmatrix} \tag{5.1}$$

Nonlinear state equations that are formed using the equations in the previous chapter are linearized around the hovering conditions by Taylor Series expansion. The state space representation is in the following form; [30]

$$\begin{aligned} \dot{x} &= Ax + Bu \\ y &= Cx + Du \end{aligned} \tag{5.2}$$

Where,

A is state matrix,

B is input matrix,

C is output matrix,

D is feed forward matrix.

The state and input vector are constructed in the form of;

$$u = \begin{bmatrix} PWM_{ESC1} \\ PWM_{ESC2} \\ PWM_{ESC3} \\ PWM_{S1} \\ PWM_{S2} \\ PWM_{S3} \end{bmatrix} \tag{5.3}$$

where u is the input vector.

Matrices in the model are given below.

$$A = \begin{bmatrix} 0 & 0 & 0 & 1 & 0 & 0 & 0 & 0 \\ 0 & 0 & 0 & 0 & 1 & 0 & 0 & 0 \\ 0 & 0 & 0 & 0 & 0 & 1 & 0 & 0 \\ 0 & 0 & 0 & 0 & 0 & 0 & 0 & 0 \\ 0 & 0 & 0 & 0 & 0 & 0 & 0 & 0 \\ 0 & 0 & 0 & 0 & 0 & 0 & 0 & 0 \\ 0 & 0 & 0 & 0 & 0 & 0 & 0 & 0 \\ 0 & 0 & 0 & 0 & 0 & 0 & 1 & 0 \end{bmatrix} \tag{5.4}$$

$$B = \begin{bmatrix} 0 & 0 & 0 & 0 & 0 & 0 \\ 0 & 0 & 0 & 0 & 0 & 0 \\ 0 & 0 & 0 & 0 & 0 & 0 \\ -110.1104 & -110.1104 & 220.2209 & -2.0846 & -2.0846 & 4.1691 \\ -190.7169 & 190.7169 & 0 & -3.6106 & 3.6106 & 0 \\ -5.1654 & -5.1654 & -5.1654 & 46.0670 & 46.0670 & 46.0670 \\ 27.7791 & 27.7791 & 27.7791 & 0 & 0 & 0 \\ 0 & 0 & 0 & 0 & 0 & 0 \end{bmatrix} \tag{5.5}$$

$$C = \begin{bmatrix} 1 & 0 & 0 & 0 & 0 & 0 & 0 & 0 \\ 0 & 1 & 0 & 0 & 0 & 0 & 0 & 0 \\ 0 & 0 & 1 & 0 & 0 & 0 & 0 & 0 \\ 0 & 0 & 0 & 0 & 0 & 0 & 0 & 1 \end{bmatrix} \quad (5.6)$$

$$D = \begin{bmatrix} 0 & 0 & 0 & 0 & 0 & 0 \\ 0 & 0 & 0 & 0 & 0 & 0 \\ 0 & 0 & 0 & 0 & 0 & 0 \\ 0 & 0 & 0 & 0 & 0 & 0 \end{bmatrix} \quad (5.7)$$

5.2 LQR Design and Simulations

Before designing the controller, basic controllability analysis is done in MATLAB. Controllability of the systems can be checked considering the rank of the following controllability matrix;

Controllability:

$$\text{rank}(\text{B AB } \text{A}^2\text{B } \text{A}^3\text{B } \text{A}^4\text{B } \text{A}^5\text{B } \text{A}^6\text{B } \text{A}^7\text{B } \text{A}^8\text{B } \text{A}^9\text{B } \text{A}^{10}\text{B } \text{A}^{11}\text{B}) = 12 \quad (5.8)$$

Cost function to be minimized is given below [1, 26, 31].

$$J = \int_0^\infty (x^T Q x + u^T R u) dt$$

The feedback control law that minimizes the value of the cost function is;

$$u = -\overline{K}x \quad (5.9)$$

Where the K is; [30]

$$\overline{K} = R^{-1} B^T P \quad (5.10)$$

According to Ricatti equation, P can be found as follows [26];

$$A^T P + PA - PBR^{-1}B^T P + Q = 0 \quad (5.11)$$

In this Ricatti Differential Equation R and Q matrices can be expresses as the weighting matrices. [30]

$$Q = \begin{bmatrix} W_1 & \cdots & 0 \\ \vdots & \ddots & \vdots \\ 0 & \cdots & Wn \end{bmatrix} \tag{5.12}$$

$$R = \begin{bmatrix} IW_1 & \cdots & 0 \\ \vdots & \ddots & \vdots \\ 0 & \cdots & IWn \end{bmatrix} \tag{5.13}$$

Where

W_i is weighting coefficient of each state,

IW_i is weighting coefficient of each input.

8 states are augmented with 4 additional error states and a regulator is designed for this new augmented system. Pitch, roll, yaw angles, and z_e position are the outputs of the system.

$$y = \begin{bmatrix} \theta \\ \phi \\ \psi \\ z_e \end{bmatrix} \tag{5.14}$$

Reference angles are;

$$R = \begin{bmatrix} R_\theta \\ R_\phi \\ R_\psi \\ R_{Z_e} \end{bmatrix} \tag{5.15}$$

Error is defined as; for each output [1].

$$e_i = R_i - y_i \tag{5.16}$$

State equations for new states are given below;

$$\dot{x}_I = e = R - y = R - Cx \tag{5.17}$$

Augmented state vector is given as below;

$$\bar{x} = \begin{bmatrix} x \\ x_I \end{bmatrix} \tag{5.18}$$

State equations for the augmented state vector are given below. [30]

$$\dot{\bar{x}} = \begin{bmatrix} \dot{x} \\ \dot{x}_I \end{bmatrix} = \begin{bmatrix} A & 0 \\ -C & 0 \end{bmatrix} \begin{bmatrix} x \\ x_I \end{bmatrix} + \begin{bmatrix} B \\ 0 \end{bmatrix} u + \begin{bmatrix} 0 \\ I \end{bmatrix} R \tag{5.19}$$

The controller schematic of the system is shown in Figure 32.

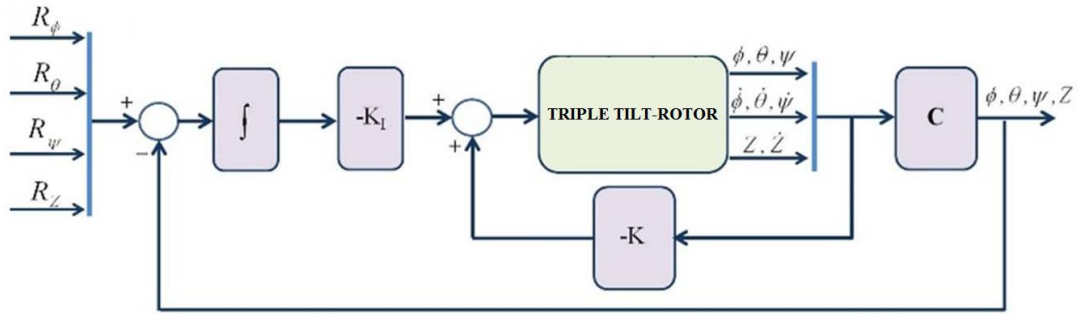

Figure 32: Schematic of the Controller

$\bar{K}$ gain matrix is calculated using MATLAB, Control System Toolbox. The augmented gains separated into K_I gain. Normalized weighting matrices, Q and R, are used.

$$Q = \begin{bmatrix} \frac{\alpha_1^2}{(x_1)_{max}^2} & & & \\ & \frac{\alpha_2^2}{(x_2)_{max}^2} & & \\ & & \ddots & \\ & & & \frac{\alpha_n^2}{(x_n)_{max}^2} \end{bmatrix} \tag{5.20}$$

$$R = \rho \begin{bmatrix} \frac{\beta_1^2}{(u_1)_{max}^2} & & & \\ & \frac{\beta_2^2}{(u_2)_{max}^2} & & \\ & & \ddots & \\ & & & \frac{\beta_m^2}{(u_m)_{max}^2} \end{bmatrix} \tag{5.21}$$

The $(x_i)_{max}$ and $(u_i)_{max}$ shows the largest desired amplitude/control input for that component of the state/actuator signal. Sum of α_i^2 s and β_i^2 s must be equal to 1 as follows:

$$\sum_i \alpha_i^2 = 1 \tag{5.22}$$

$$\sum_i \beta_i^2 = 1 \tag{5.23}$$

ρ is used as the last relative weighting between the control and state penalties. The allowed state range $(x_i)_{max}$ for $Q_{1,1}$, $Q_{2,2}$ are ±5 degrees and for $Q_{3,3}$ is ±10 degrees. Also, the allowed state range $(x_i)_{max}$ for $Q_{10,10}$, $Q_{11,11}$ are ±0.1 meters and for $Q_{12,12}$ is ±0.05 meters. According to these limitations for calculating Q and R matrices take form as following;

$$Q = \begin{bmatrix} 7.295 & 0 & 0 & 0 & 0 & 0 & 0 & 0 & 0 & 0 & 0 & 0 \\ 0 & 7.295 & 0 & 0 & 0 & 0 & 0 & 0 & 0 & 0 & 0 & 0 \\ 0 & 0 & 1.824 & 0 & 0 & 0 & 0 & 0 & 0 & 0 & 0 & 0 \\ 0 & 0 & 0 & 7.295 & 0 & 0 & 0 & 0 & 0 & 0 & 0 & 0 \\ 0 & 0 & 0 & 0 & 7.295 & 0 & 0 & 0 & 0 & 0 & 0 & 0 \\ 0 & 0 & 0 & 0 & 0 & 1.824 & 0 & 0 & 0 & 0 & 0 & 0 \\ 0 & 0 & 0 & 0 & 0 & 0 & 5.556 & 0 & 0 & 0 & 0 & 0 \\ 0 & 0 & 0 & 0 & 0 & 0 & 0 & 22.222 & 0 & 0 & 0 & 0 \\ 0 & 0 & 0 & 0 & 0 & 0 & 0 & 0 & 7.295 & 0 & 0 & 0 \\ 0 & 0 & 0 & 0 & 0 & 0 & 0 & 0 & 0 & 7.295 & 0 & 0 \\ 0 & 0 & 0 & 0 & 0 & 0 & 0 & 0 & 0 & 0 & 1.824 & 0 \\ 0 & 0 & 0 & 0 & 0 & 0 & 0 & 0 & 0 & 0 & 0 & 22.222 \end{bmatrix} \tag{5.24}$$

$$R = \begin{bmatrix} 66.67 & 0 & 0 & 0 & 0 & 0 \\ 0 & 66.67 & 0 & 0 & 0 & 0 \\ 0 & 0 & 66.67 & 0 & 0 & 0 \\ 0 & 0 & 0 & 416.67 & 0 & 0 \\ 0 & 0 & 0 & 0 & 416.67 & 0 \\ 0 & 0 & 0 & 0 & 0 & 416.67 \end{bmatrix} \tag{5.25}$$

New K and KI matrices are illustrated below.

$$K = \begin{bmatrix} -0.2354 & -0.4077 & -0.0109 & -0.1377 & -0.2384 & -0.0063 & 0.1987 & 0.4928 \\ -0.2354 & 0.4077 & -0.0109 & -0.1377 & 0.2384 & -0.0063 & 0.1987 & 0.4928 \\ 0.4708 & 0 & -0.0109 & 0.2753 & 0 & -0.0063 & 0.1987 & 0.4928 \\ -0.0007 & -0.0012 & 0.0726 & -0.0004 & -0.0007 & 0.0500 & 0.0076 & 0.0145 \\ -0.0007 & 0.0012 & 0.0726 & -0.0004 & 0.0007 & 0.0500 & 0.0076 & 0.0145 \\ 0.0014 & 0 & 0.0726 & 0.0008 & 0 & 0.0500 & 0.0076 & 0.0145 \end{bmatrix} \tag{5.26}$$

$$K_I = \begin{bmatrix} 0.1350 & 0.2339 & 0.0063 & -0.3326 \\ 0.1350 & -0.2339 & 0.0063 & -0.3326 \\ -0.2701 & 0 & 0.0063 & -0.3326 \\ 0.0004 & 0.0007 & -0.0381 & -0.0088 \\ 0.0004 & -0.0007 & -0.0381 & -0.0088 \\ -0.0008 & 0 & -0.0381 & -0.0088 \end{bmatrix} \tag{5.27}$$

The block diagram of the control algorithm is done in Simulink and required parameters are taken from MATLAB workspace. The Simulink block diagram of the system is illustrated below in Figure 32. As shown, state-space model and non-linear model tested with the algorithm. When the input references are given to each state, outputs of the model are drawn into graph with its input references. Operating points added to non-linear system inputs. Also, initial conditions of the system are applied to the non-linear model. Units are degree for roll, pitch, yaw angle, meters for ze in the graphs respectively.

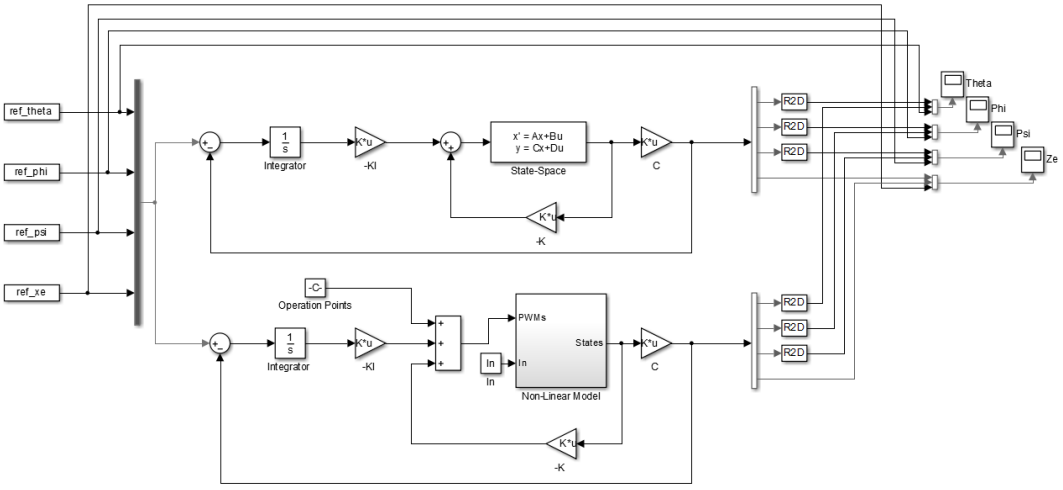

Figure 33: Block Diagram of the Control Algorithm

Pitch, roll and yaw control outputs are given below:

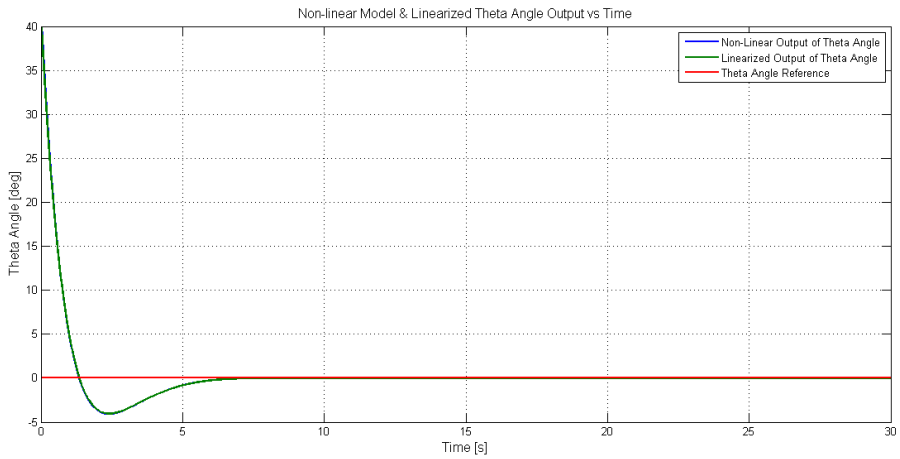

Figure 34: Pitch Angle Control with reference in simulation

As shown in pitch graph, the first graph of the Figure 34 is non-linear model theta output and the second one is state space model output. All models have a 0 reference and the initial position of the pitch angle is 40 degree. As seen in Figure 33, the pitch angle has been stabilized.

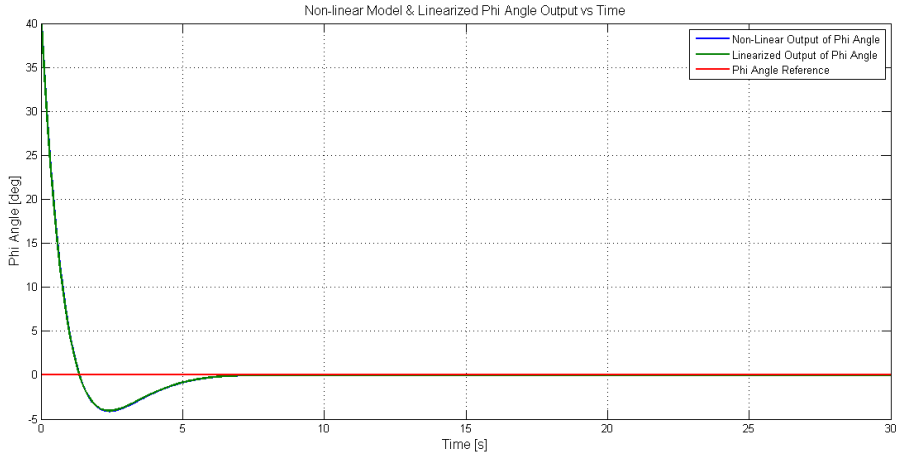

Figure 35: Roll Angle Control with reference in simulation

As same as the pitch graphs; roll angle, 40 degree initial condition stabilized roll angle nearly at the same time. Roll and pitch have similar dynamics, that's why Figure 36 as same as Figure 35.

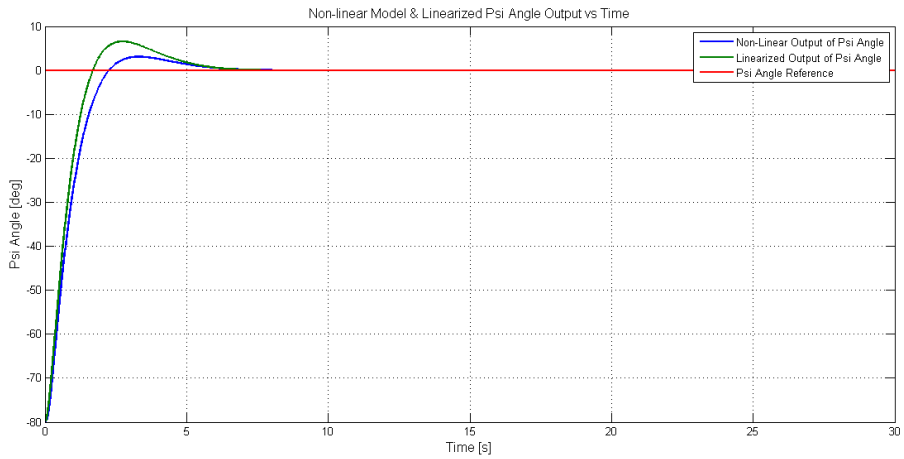

Figure 36: Yaw Angle Control with reference in simulation

As shown in Figure 36, yaw angle stabilizes in almost five seconds. The initial condition of yaw angle is -80 degree. Altitude control output is shown in Figure 37.

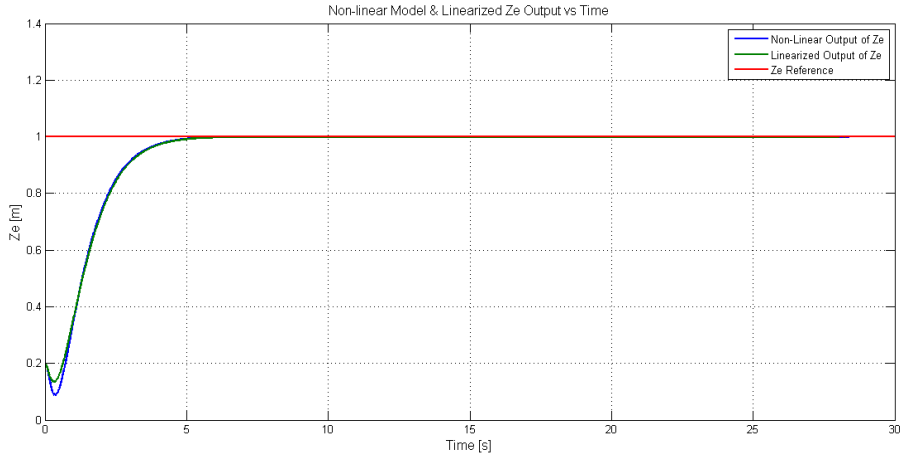

Figure 37: Altitude Control with reference in simulation

As shown in altitude graph in Figure 37, altitude stabilized. The initial altitude of the system is 0.2 meters because of the landing gears.

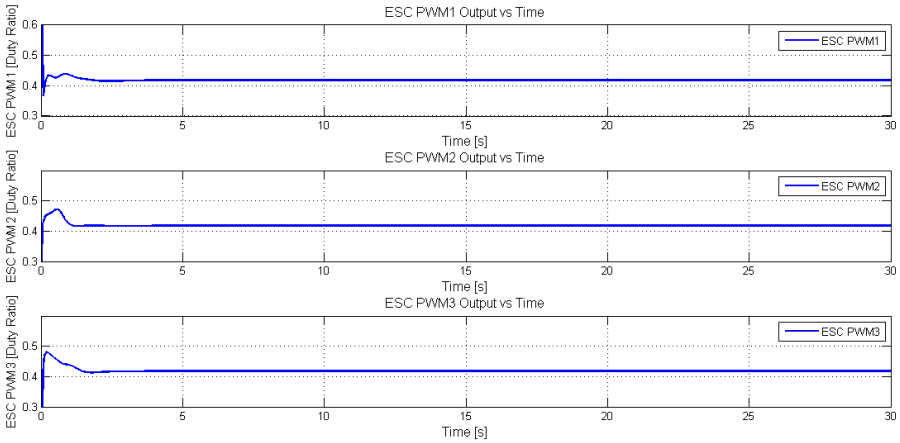

Figure 38: ESC PWM Duty Raito Values in Simulation

The nominal (PWM needed for hovering) PWM duty ratios of the ESCs are 0.4224. This nominal PWM value calculated with the power needed to hover the system. The ranges of the PWM signal are between 30% and 60% duty cycle. As shown in the Figure 38, the controller outputs are in the range of operation.

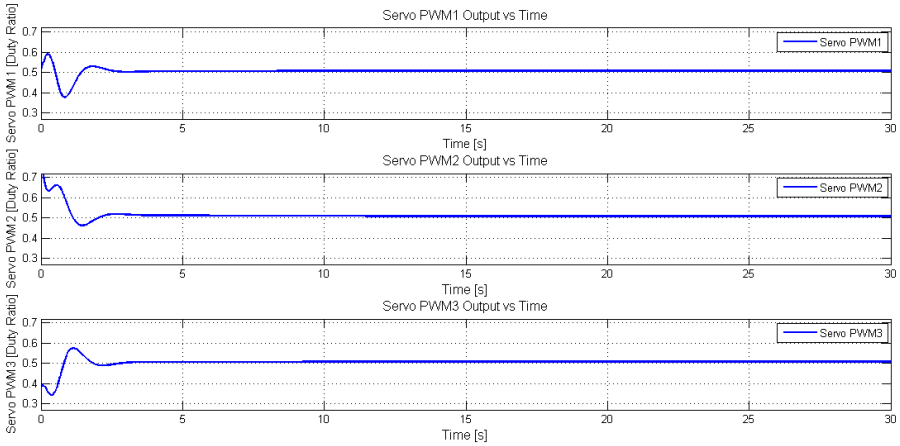

Figure 39: Servo PWM Duty Ratios in simulation

Like ESC PWM duty ratios the nominal value of the servo motors are 0.495, which means alpha angles are 0. The range of the PWM duty ratios are between 0.27 and 0.72. Similar to previous PWM duty ratios, servo duty ratios are in the range also.

5.3 Real-Time Tests

After the simulations are done successfully, RT tests are started. Instead of the steady-space model, sensor inputs and PWM outputs are connected to the control algorithm. Q and R matrices and operating points are revised. The inside of the model is shown in Figure 40. Roll, pitch, yaw angles and z_e were directly taken from the sensor. For z_e, an analog low pass filter is used [31].

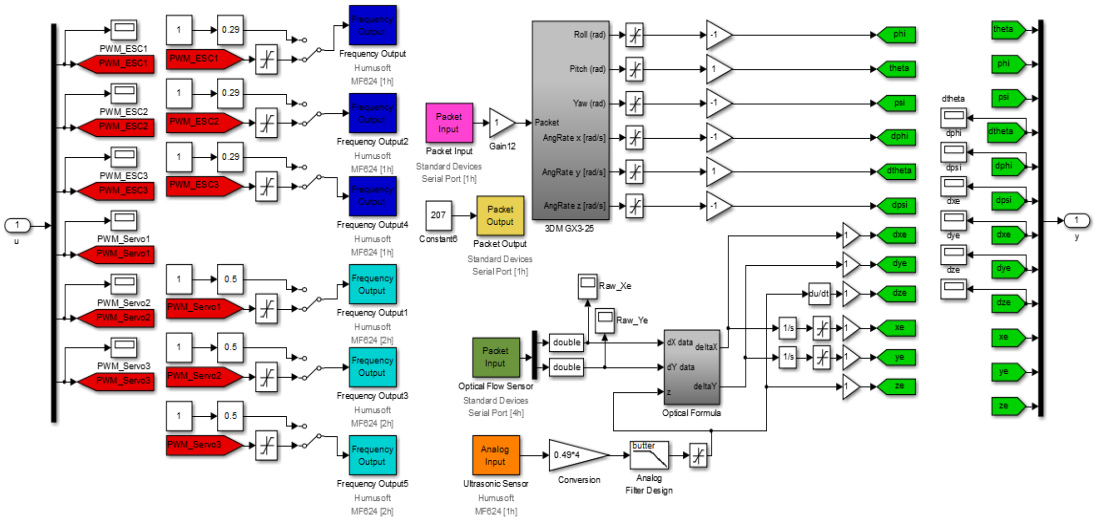

Figure 40: RT Simulink Block Diagram – Inside of the Model

Outputs of optical flow sensor are just used to monitor the translational motion. The controller is tuned as follows and same steps to get K and K_I gains are applied.

$$Q = \begin{bmatrix} 5 & 0 & 0 & 0 & 0 & 0 & 0 & 0 & 0 & 0 & 0 & 0 \\ 0 & 5 & 0 & 0 & 0 & 0 & 0 & 0 & 0 & 0 & 0 & 0 \\ 0 & 0 & 5 & 0 & 0 & 0 & 0 & 0 & 0 & 0 & 0 & 0 \\ 0 & 0 & 0 & 1 & 0 & 0 & 0 & 0 & 0 & 0 & 0 & 0 \\ 0 & 0 & 0 & 0 & 1 & 0 & 0 & 0 & 0 & 0 & 0 & 0 \\ 0 & 0 & 0 & 0 & 0 & 1 & 0 & 0 & 0 & 0 & 0 & 0 \\ 0 & 0 & 0 & 0 & 0 & 0 & 1 & 0 & 0 & 0 & 0 & 0 \\ 0 & 0 & 0 & 0 & 0 & 0 & 0 & 1 & 0 & 0 & 0 & 0 \\ 0 & 0 & 0 & 0 & 0 & 0 & 0 & 0 & 2 & 0 & 0 & 0 \\ 0 & 0 & 0 & 0 & 0 & 0 & 0 & 0 & 0 & 2 & 0 & 0 \\ 0 & 0 & 0 & 0 & 0 & 0 & 0 & 0 & 0 & 0 & 0.1 & 0 \\ 0 & 0 & 0 & 0 & 0 & 0 & 0 & 0 & 0 & 0 & 0 & 1 \end{bmatrix} \tag{5.28}$$

$$R = \begin{bmatrix} 1250 & 0 & 0 & 0 & 0 & 0 \\ 0 & 1250 & 0 & 0 & 0 & 0 \\ 0 & 0 & 1250 & 0 & 0 & 0 \\ 0 & 0 & 0 & 500 & 0 & 0 \\ 0 & 0 & 0 & 0 & 500 & 0 \\ 0 & 0 & 0 & 0 & 0 & 500 \end{bmatrix} \quad (5.29)$$

New K and K_I matrices are illustrated below.

$$K = \begin{bmatrix} -0.0342 & -0.0592 & -0.0021 & -0.0154 & -0.0266 & -0.001 & 0.0340 & 0.0371 \\ -0.0342 & 0.0592 & -0.0021 & -0.0154 & 0.0266 & -0.001 & 0.0340 & 0.0371 \\ 0.0684 & 0 & -0.0021 & 0.0308 & 0 & -0.001 & 0.0340 & 0.0371 \\ -0.0016 & -0.0028 & 0.0630 & -0.0007 & -0.0013 & 0.0397 & 0.0033 & 0.0033 \\ -0.0016 & 0.0028 & 0.0630 & -0.0007 & 0.0013 & 0.0397 & 0.0033 & 0.0033 \\ 0.0032 & 0 & 0.0630 & 0.0015 & 0 & 0.0397 & 0.0033 & 0.0033 \end{bmatrix} \quad (5.30)$$

$$K_I = \begin{bmatrix} 0.0163 & 0.0283 & 0.0003 & -0.0163 \\ 0.0163 & -0.0283 & 0.0003 & -0.0163 \\ -0.0326 & 0 & 0.0003 & -0.0163 \\ 0.0008 & 0.0013 & -0.0082 & -0.0014 \\ 0.0008 & -0.0013 & -0.0082 & -0.0014 \\ -0.0015 & 0 & -0.0082 & -0.0014 \end{bmatrix} \quad (5.31)$$

All connections of the system are established before the flight tests. Security precautions for the tests are also completed. Net and sponge are placed and the system is tied to the ground for security. The test area of the system is shown in Figure 41.

Figure 41: Test Area

First RT test is the attitude and altitude control of the system. Roll, pitch, yaw and altitude states are stabilized. In order to achieve this, pitch angle, roll angle and their angular rates are controlled. Pitch angle and zero reference shown in Figure 42 and Figure 43, roll and yaw angle are shown respectively.

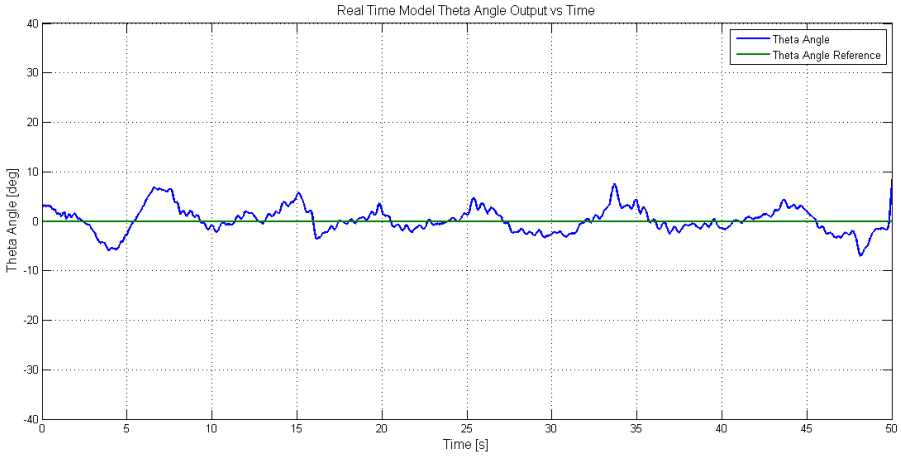

Figure 42: Pitch Angle Control with reference in real model

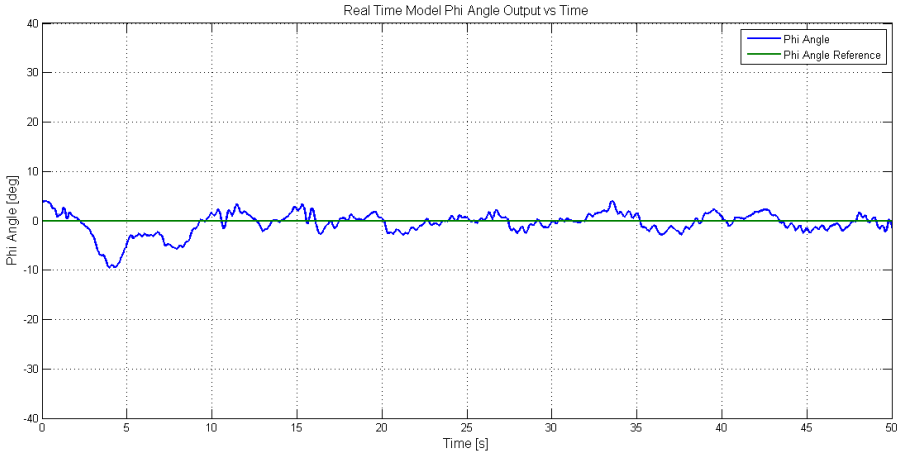

Figure 43: Roll Angle Control with reference in real model

After stabilizing pitch and roll axis, yaw angle and its angular rate are controlled. Yaw axis stabilization is shown in Figure 44.

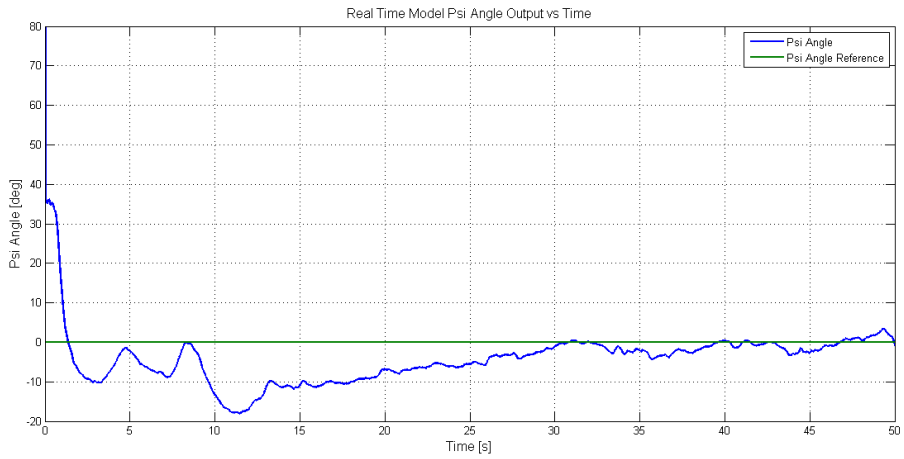

Figure 44: Yaw Angle Control with reference in simulation

After yaw angle stabilization, the attitude dynamics are stabilized. The altitude of the system is controlled using 0.7m reference which increased from 0.2m to 0.7m in 5s. The output of the test is shown in Figure 45.

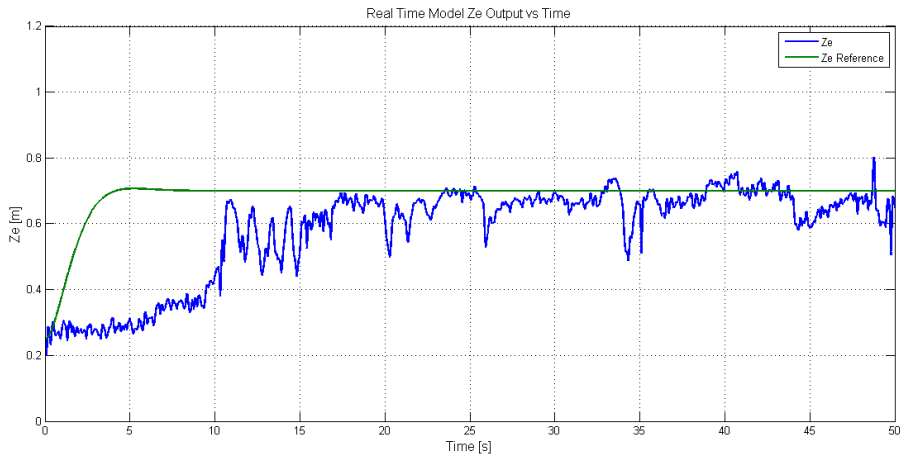

Figure 45: Altitude Control with reference in real model

The altitude control of the system is slower than the other dynamics because of the related element of weighting matrix is smaller than others. As shown in Figure 46, the system stabilized with a small steady state error. The inputs of the system are shown in Figure 46.

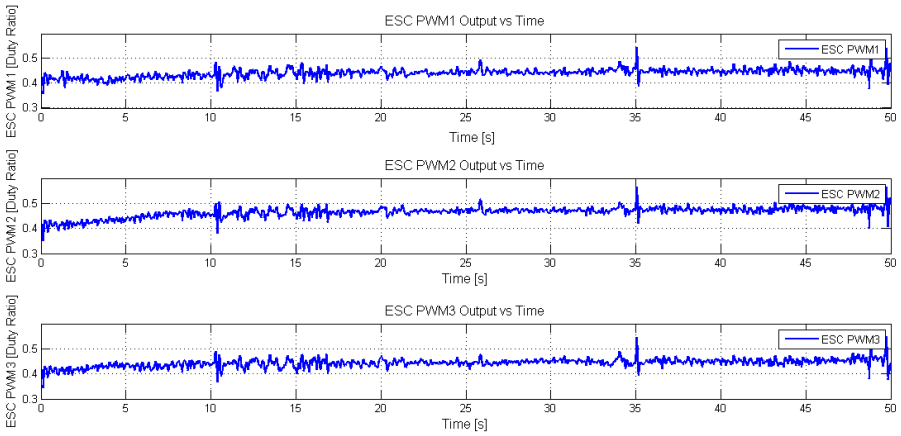

Figure 46: ESC PWM Outputs in real model

As in the simulation, the nominal PWM duty ratios of the ESCs are 0.4224. As in the simulations, the controller outputs are not saturated in RT experiments. According to the Figure 46 above the controller outputs are not saturated.

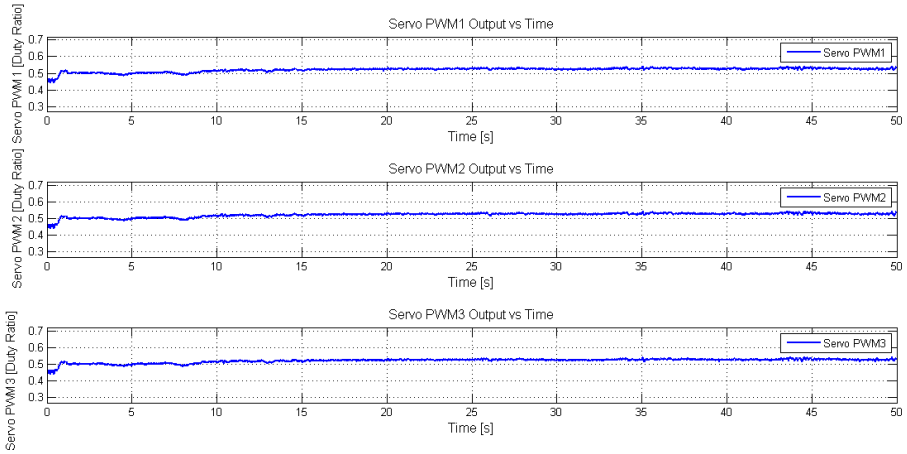

Figure 47: Servo PWM Outputs in simulation

Like ESC PWM duty ratios and simulations the nominal value of the servo motors are 0.495 which means 0 degree. The limits of the system are between 0.27 and 0.72. Similar to previous PWM duty ratios, servo duty ratios are not saturated also.

Figure 48: Flying System

As shown in Figure 48 above, snapshots of the system on ground and during flight tests are shown. From the graphs above triple tilt-rotor system is stabilized with LQR controller.

CHAPTER 6

DISCUSSION AND CONCLUSION

In essence, triple tilt-rotor unmanned aerial vehicle is designed, manufactured, simulated and tested as stated in previous chapters. The novel design, triple tilt-rotor, has a different structure from the structures stated in literature. The structure is combination of Y-shaped and delta-shaped chasses; it decreases the disturbances coming from bending and vibration. On the system, BLDC and servo motor are used as actuators and IMU, ultrasonic proximity sensor and optical flow sensor are used as sensors of the system. The IMU and BLDC motors placed with anti-vibration pins to the CF bars and ABS parts. Adding these features to the structure, improves the robustness. Before simulations, mathematical modeling of the system was studied with Newton-Lagrange method. Simulations are completed using MATLAB & Simulink. In simulation roll, pitch, yaw angles, and altitude are stabilized and in RT tests roll, pitch, yaw angles, and altitude are stabilized using 8 states model. Also, the mathematical model based on Newton-Lagrange method is verified with the real system. As stated in Chapter 5, LQR controller gains have been calculated for combination of the states and augmented states. MATLAB, Control System Toolbox is used for calculating controller gains using Q and R weighting matrices. Use of normalized gain matrices has advantages. During real-time tests some tuning effort is needed to get desired response from the system. The augmented gains multiplied by augmented states after integral action for rejecting steady state errors. After system is successfully simulated, real system tests are finished. Because of the assumptions and non-considered details, controller gains re-tuned during RT tests. These details are estimated unknown parameters of model, sampling time, limitations, cable effect, ground effect and sensor noises.

To conclude, using LQR controller with integral action is designed for stabilizing attitude and altitude dynamics. The controller is designed based on obtained linearized mathematical model. Implementation of the LQR for the simulation of linearized and non-linear model is completed and the system is successfully stabilized for attitude and altitude. Also, attitude and altitude are successfully stabilized in RT tests. According to the results, the aim of the thesis is achieved.

Integration of optical flow in state feedback will make us control the translational motion in ground XY plane. Sensor fusion will be studied for the optical flow sensor, IMU and proximity sensor. Designed normalized LQR control architecture will be extended to translational control also.

REFERENCES

[1] A. Güçlü, 2012, "Attitude and Altitude Control of an Outdoor Quadrotor", M.S. Thesis, Mechatronics Engineering Department, Atılım University, Ankara, Turkey

[2] K. T. Öner, E. Çetinsoy, M. Ünel, M. F. Akşit, İ. Kandemir, K. Gülez, 2009, "Dynamic Model and Control of a New Quadrotor Unmanned Aerial Vehicle with Tilt-Wing Mechanism", *International Journal of Applied Science, Engineering & Technology*, Vol. 5 Issue 2, p: 133

[3] "Comco Ikarus C42B", Web, 3 Jul 2013, http://www.comco-ikarus.de/Pages/produkte-comco/c-42b-ul.php?lang=en

[4] "Agusta Westland AW109 Power" Web, 3 Jul 2013, http://www.agustawestland.com/product/aw109-power-0

[5] I. J. Rimson, L. Benner, 2008, "The Sky Isn't Falling – Or Is It? Part 1", *Journal of System Safety*, p: 4-7, Unionville, U.S.A.

[6] J. Escareno, A. Sanchez, O. Garcia, R. Lozano, 2008, "Triple Tilting Rotor mini-UAV: Modeling and Embedded Control of the Attitude", *American Control Conference 2008*, p: 3476-3481, Seattle, Washington, U.S.A.

[7] D. W. Yoo, H. D. Oh, D. Y. Won, M. J. Tahk, 2010, "Dynamic Modeling and Stabilization Techniques for Tri-Rotor Unmanned Aerial Vehicles", *International Journal of Aeronautical and Space Sciences*, p: 167-174

[8] S. Salazar-Cruz, F. Kendoul, R. Lozano, I. Fantoni, 2006, "Real-Time Control of a Small-Scale Helicopter Having Three Rotors", *International Conference on Intelligent Robots and Systems*, p: 2924-2929, Beijing, China

[9] S. Salazar-Cruz, R. Lozano, 2005, "Stabilization and nonlinear control for a novel trirotor mini-aircraft", *International Conference on Robotics and Automation*, p: 2612-2617, Barcelona, Spain

[10] H. Alwafi, 2013, "Attitude and Altitude Control of Two Wheel Trirotor Hybrid Robot", M.S. Thesis, Mechatronics Engineering Department, Atılım University, Ankara, Turkey

[11] S. Yoon, S. J. Lee, B. Lee, C. J. Kim, Y. J. Lee, S. Sung, 2013, "Design and Flight Test of a Small Tri-Rotor Unmanned Vehicle with a LQR Based Onboard Attitude Control System", *International Journal of Innovative Computing, Information and Control*, p: 2347-2360, Kumamoto, Japan

[12] M. Ryll, H. H. Bülthoff, P. R. Giordano, 2012, "Modeling and Control of a Quadrotor UAV with Tilting Propellers", *IEEE International Conference on Robotics and Automation*, p: 4606-4613, Minnesota, USA

[13] F. Kendoul, I. Fantoni, R. Lozano, 2005, "Modeling and control of a small autonomous aircraft having two tilting rotors", *44th IEEE Conference on Decision and Control, and the European Control Conference*, p: 8144-8149, Seville, Spain

[14] E. B. Nice, 2004, "Design of a Four Rotor Hovering Vehicle", M.S. Thesis, Cornell University, New York, U.S.A.

[15] S. Bouabdallah, 2007, "Design and Control of Quadrotors with Application to Autonomous Flying", M.S. Thesis, École Polytechnique Fédérale de Lausanne, Lausanne, Switzerland

[16] P. Pounds, R. Mahony, P. Hynes, J. Roberts, 2002, "Design of a Four-Rotor Aerial Robot", *Australasian Conference on Robotics and Automation*, p: 145-150, Auckland, New Zealand

[17] M. C. Achtelik, K. M. Doth, D. Gurdan, J. Stumpf, 2012, "Design of a Multi Rotor MAV with regard to Efciency, Dynamics and Redundancy", *AIAA Guidance, Navigation, and Control Conference*, p: 1-17, Minnesota, U.S.A.

[18] P. Pounds, R. Mahony, P. Corke, 2010, "Modelling and Control of a Large Quadrotor Robot", *A Journal of IFAC, the International Federation of Automatic Control*, p:691-699, Laxenburg, Austria

[19] V. Kelly, 2004, "Carbon Fiber: Manufacture and Applications," Kidlington, Oxford, UK ; New York, USA

[20] M. Wallace, 2010, Web, 3 Jul 2013, http://www.rcgroups.com/forums/showpost.php?p=15457394&postcount=567

[21] D. Cook, 2007, Web, 3 Jul 2013, http://www.rcgroups.com/forums/showpost.php?p=8712197&postcount=3

[22] "Pro Tricopter Delrin Kit v1.2", Web, 3 Jul 2013, http://www.fpvmanuals.com/tricopter/

[23] C. McGrath, D. Uhlig, E. Eaton, J. Brandt, K. Joye, K. Tehrani, O. Shetty, P. Gush, R. Deters, 2012 "UIUC Propeller Database", Web, 3 Jul 2013, http://www.ae.illinois.edu/m-selig/props/propDB.html

[24] "3DM-GX3 ® -25 Data Communications Protocol.", 2012, Web. 3 Jul 2013, http://files.microstrain.com/3DM-GX3-Data-Communications-Protocol.pdf

[25] "Optical Flow Sensor", Web, 3 Jul 2013, https://code.google.com/p/arducopter/wiki/AC2_OptFlow

[26] D. Küçük, 2010, "Design Of Two Wheeled Twin Rotored Hybrid Robotic Platform", M.S. Thesis, Mechatronics Engineering Department, Atılım University, Ankara, Turkey

[27] U. L. Ly, 1997, "Stability and Control of Flight Vehicle", Department of Aeronautics and Astronautics, University of Washington, Seattle, U.S.A.

[28] B. Etkin, L. D.Reid, 1996, "Dynamics of Flight: Stability and Control 3rd Edition", Wiley

[29] Y. Bestaoui, S. Hima, C. Sentouh, 2003, "Motion Planning of a Fully Actuated Unmanned Air Vehicle", *AIAA Guidance, Navigation, and Control Conference and Exhibit*, p: 1-11 Texas, U.S.A

[30] K. Ogata, "Modern Control Engineering 3rd Edition", University of Minnesota, pp. 151 – 152

[31] A. Rys, R. Czyba, G. Szafranski, "Practical Aspects of Trirotor MAV Development", 2011, *Proceedings of the International Micro Air Vehicles Conference 2011 Summer Edition*, p: 64-69, Harde, The Netherlands

APPENDIX A

Publications during the San-Tez Project:

[1] K. B. Arıkan, B. İrfanoğlu, A. Kaçar, M. Yıldız, 2011, "Attitude Stabilization of a Novel Flying Robot by Dynamic Compensation", *6. Ankara International Aerospace Conference*, Ankara, Turkey

[2] A. Kaçar, B. Tok, A. C. Kahvecioğlu, O. Albostan, S. Köse, B. İrfanoğlu, K. B. Arıkan, 2012, "Üç Dönerkanatlı ve Döner-Rotorlu İnsansız Hava Aracının Tasarımı", *6.Savunma Teknolojileri Kongresi, SAVTEK-2012,* Ankara, Turkey

[3] O. Albostan, A. Kaçar, B. Tok, A. C. Kahvecioğlu, S. Köse, B. İrfanoğlu, K. B. Arıkan, 2012, "Üç Döner Rotorlu İnsansız Hava Aracının Modellenmesi ve Kontrolü", *Otomatik Kontrol Türk Milli Komitesi 2012 Ulusal Toplantısı*, Niğde, Turkey

[4] A. Kaçar, S. Köse, 2012, "İnsansız Hava Aracı için Benzetim Ortamında Gerçek Zamanlı Oto-Pilot Tasarımı", *IV. Ulusal Havacılık ve Uzay Konferansı,* p:072,1-6, İstanbul, Turkey

APPENDIX B

1. Complete Technical Drawing

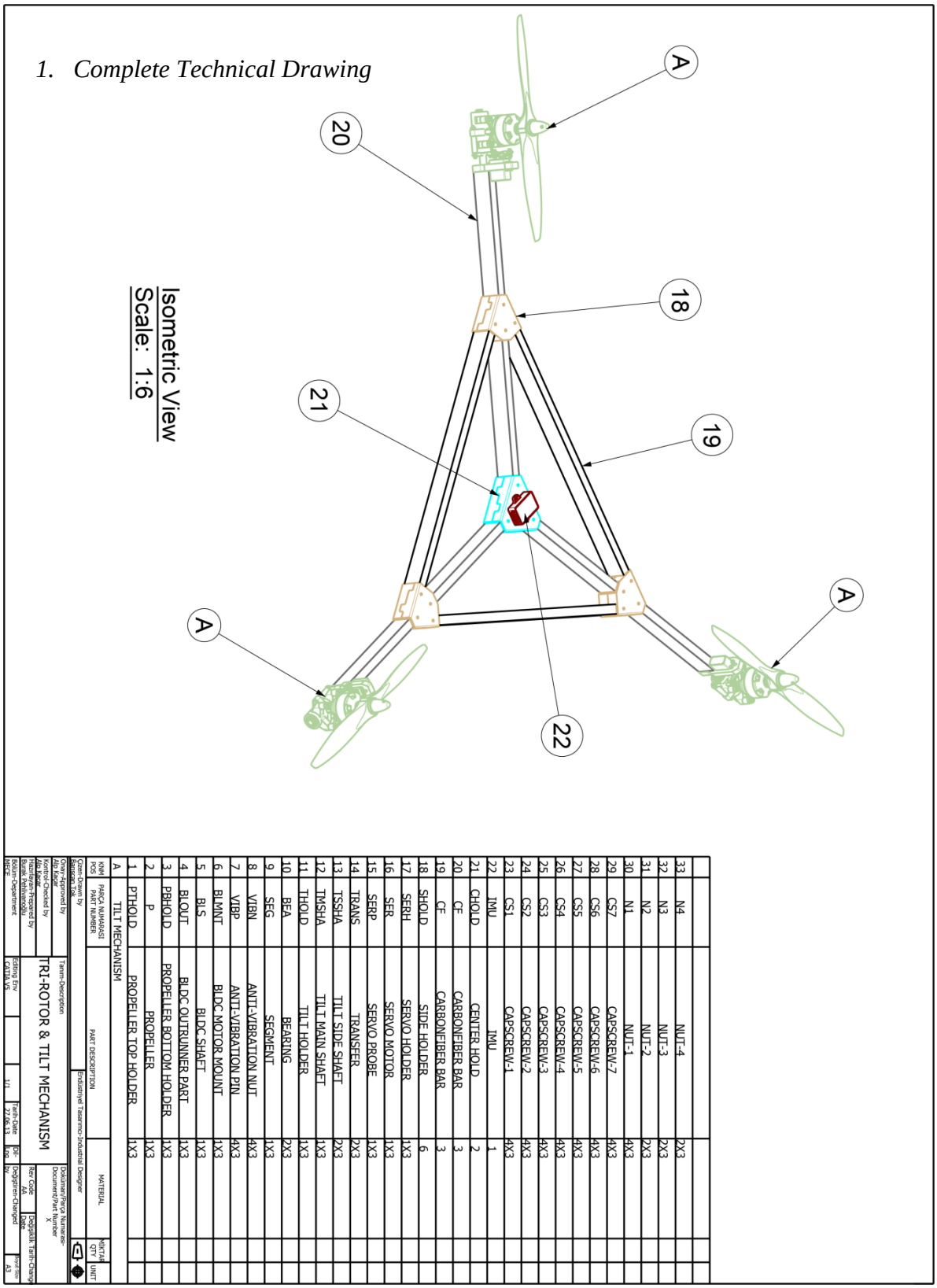

33	N4	NUT-4	2X3	
32	N3	NUT-3	2X3	
31	N2	NUT-2	2X3	
30	N1	NUT-1	4X3	
29	CS7	CAPSCREW-7	4X3	
28	CS6	CAPSCREW-6	4X3	
27	CS5	CAPSCREW-5	4X3	
26	CS4	CAPSCREW-4	4X3	
25	CS3	CAPSCREW-3	4X3	
24	CS2	CAPSCREW-2	4X3	
23	CS1	CAPSCREW-1	4X3	
22	IMU	IMU	1	
21	CHOLD	CENTER HOLD	2	
20	CF	CARBONFIBER BAR	3	
19	CF	CARBONFIBER BAR	3	
18	SHOLD	SIDE HOLDER	6	
17	SERH	SERVO HOLDER	1X3	
16	SER	SERVO MOTOR	1X3	
15	SERP	SERVO PROBE	1X3	
14	TRANS	TRANSFER	2X3	
13	TSSHA	TILT SIDE SHAFT	2X3	
12	TMSHA	TILT MAIN SHAFT	1X3	
11	THOLD	TILT HOLDER	1X3	
10	BEA	BEARING	2X3	
9	SEG	SEGMENT	1X3	
8	VIBN	ANTI-VIBRATION NUT	4X3	
7	VIBP	ANTI-VIBRATION PIN	4X3	
6	BLMNT	BLDC MOTOR MOUNT	1X3	
5	BLS	BLDC SHAFT	1X3	
4	BLOUT	BLDC OUTRUNNER PART	1X3	
3	PBHOLD	PROPELLER BOTTOM HOLDER	1X3	
2	P	PROPELLER	1X3	
1	PTHOLD	PROPELLER TOP HOLDER	1X3	
A	TILT MECHANISM			
KNM POS	PARÇA NUMARASI PART NUMBER	PART DESCRIPTION	MATERIAL	MİKTAR QTY

Çizen-Drawn by: Endüstriyel Tasarımcı-Industrial Designer
Kontrol-Checked by: Alp Kaçar
Hazırlayan-Prepared by: Burak Pehlivanoğlu
Bölüm-Department: Makine

Tasarım-Description: TRI-ROTOR & TILT MECHANISM
Editörlü Env: CATIA V5
Ölçü: 1/1
Tarih-Date: 27.06.13
Dökümün/Parça Numarası-Document/Part Number: X
Rev. Code: AA
Değiştiren-Changed by:
Değişiklik Tarihi-Change Date:
Boyut-Size: A3
Dir. No:

2. Tilt Mechanism Assembly